A DSP-BASED POSTDISTORTION RECEIVER

by

Le Dinh Quach

B.A.Sc., Simon Fraser University, 1991

A THESIS SUBMITTED IN PARTIAL FULFILLMENT

OF THE REQUIREMENTS FOR THE DEGREE OF

MASTER OF APPLIED SCIENCE

in the School of Engineering Science

SIMON FRASER UNIVERSITY

December 1992

APPROVAL

Name: Le Dinh Quach

Degree: Master of Applied Science (Engineering Science)

Title of Thesis: A DSP-Based Postdistortion Receiver

Dr. John Jones, PEng
Associate Professor
School of Engineering Science, SFU

Examining Committee:

Chairman:

Dr. John Jones, PEng
Associate Professor
School of Engineering Science, SFU

Senior Supervisor:

Dr. Shawn P. Stapleton, PEng
Associate Professor
School of Engineering Science, SFU

Supervisor:

Dr. James K. Cavers, PEng
Director
School of Engineering Science, SFU

Committee Member:

Dr. Jacques Vaisey
Assistant Professor
School of Engineering Science, SFU

Date Approved: December, 11, 1992

PARTIAL COPYRIGHT LICENSE

I hereby grant to Simon Fraser University the right to lend my thesis, project or extended essay (the title of which is shown below) to users of the Simon Fraser University Library, and to make partial or single copies only for such users or in response to a request from the library of any other university, or other educational institution, on its own behalf or for one of its users. I further agree that permission for multiple copying of this work for scholarly purposes may be granted by me or the Dean of Graduate Studies. It is understood that copying or publication of this work for financial gain shall not be allowed without my written permission.

Title of Thesis/Project/Extended Essay

A DSP-based Postdistortion Receiver

Author:

(signature)

Le D. Quach

(name)

Dec 14, 1992

(date)

ABSTRACT

This thesis presents a novel *Postdistortion* receiver, for possible future mobile communication systems, which can increase both the spectral efficiency and the transmitter's power efficiency (especially important for portable units). Postdistortion is a technique, implemented at the base-station receiver, to compensate for AM-AM and AM-PM nonlinearities of a transmitter's amplifier which, if uncompensated, would cause adjacent channel interference.

Three main contributions are given. First, analysis is presented which shows the quadratic dependence of the adjacent-channel interference power on both the amplifier and postdistorter coefficients. The quadratic function ensures a global minimum that can be found with an optimization algorithm. Second, a unique adaptation method is derived which can iteratively adapt the postdistorter coefficients, without an interruption for a training period, for slow variations in the transmitter amplifier's characteristics. Third, various aspects of system performance, including SNR and convergence speed, are simulated. The system performance in fading channel conditions, an inevitable problem in mobile communications, is also considered. The simulation and measured results show that the postdistortion technique can improve the out-of-band emission by up to 20 dB with 5-dB OBO; the corresponding increase in mobile transmitter power efficiency is approximately a factor of 10. The spectral efficiency is approximately increased by 20% with the postdistortion implementation.

ACKNOWLEDGEMENTS

I would like to thank my senior supervisor Dr. Shawn Stapleton for giving me the opportunity to work on this project and also for helping and encouraging me on many occasions. I am also very grateful to my committee members, Dr. Jim Cavers and Dr. Jacques Vaisey, for their assistance and helpful hints. Also, many thanks to the people in the RF/Microwave Lab (Derek Hilborn, Wing Yu, Andy Fung, Andrew Keir, Marlo Gothe and especially Sirooj Rambaran) for their friendliness and technical aid.

DEDICATION

To my grandma, my family and My Lan with love.

TABLE OF CONTENTS

LIST OF FIGURES

LIST OF TABLES

1 INTRODUCTION

Spectral and power efficiency are two desirable design considerations in mobile data communications. Unfortunately, these two constraints are not complementary to each other. Linear modulation methods such as 16-QAM and QPSK are employed in order to improve the spectral efficiency. Consequently, class A power amplifiers are needed to ensure the performance of these modulation techniques. However, a serious drawback of class A amplifiers is their poor power efficiency. Power efficiency is especially important for portable units. To conserve battery energy in a portable unit, the transmitter must use a high power-efficient amplifier such as class AB or B amplifiers which inherently have poor linearity. Consequently, the use of nonlinear amplifiers with an amplitude modulating envelope will cause adjacent-channel interference (ACI) due to intermodulation (IM) products.

The traditional solution to this dichotomy is to linearize the transmitter's power amplifier. Linearization techniques can be categorized into five types: active biasing [1], feed-forward [2], negative feedback [2], LINC (LInear Amplification using Non-linear Components) [3], and predistortion [4-7]. These techniques can improve the IM suppression by 10 to 15 dB. All of these techniques are implemented at the transmitters; consequently, this arrangement increases the transmitters' complexity and weight which are also important factors for portable units.

A possible solution to the dichotomy above is to allow for the IM's to spill-over into the adjacent channels (potential relaxation of FCC requirements) and then perform correction at the base-station receiver [8,9]. This *Postdistortion* approach will allow for systems which have higher data rates at the same time as maintaining the portable units' power efficiency.

This thesis presents an adaptive DSP-based postdistortion receiver, for possible future mobile communications systems, which allows for an increase in spectral efficiency as well as an increase in transmitter power efficiency. The basic idea of the postdistortion technique is to compensate for the AM-AM and AM-PM nonlinearities of adjacent channel's power amplifier, at the base-station receiver. Implementing the postdistortion technique at the base station, allows all the portable transmitters to transmit with a more relaxed out-of-band emission requirements; for instance, -45 dBc rather than -60 dBc, provided that the base station will still transmit with -60 dBc out-of-band emission. Consequently, the portable transmitters can use amplifiers with a high power efficiency such as class AB or B amplifiers. Moreover, the postdistortion technique allows for a minimal guardband between adjacent channels; thereby increasing the number of possible transmission channels over an allocated frequency spectrum. Postdistortion would only be required at the base stations while all the portable transceivers can be simple, light weight and power efficient. Therefore, the increase in base-station system complexity, power consumption and cost, of implementing this postdistortion technique, can be well justified.

The postdistortion technique is a method for slowly adapting to varying amplifier characteristics. In general, adaptability is only required for drifts in the power amplifier's characteristics. These drifts are mainly caused by changes in temperature, supply voltage variations, aging of devices and switching between channels. Adaptation for these variations can be slow, with a significant reduction in complexity. Adaptation is accomplished by iterative adjustments of the postdistorter parameters to minimize the IM power.

The main objective of this thesis is to perform a feasibility study on postdistortion and to implement the system in hardware. Part of the thesis work focused on simulating an adaptive postdistortion system. Different aspects of the system performance, including the system's spectrum, signal-to-noise ratio (SNR), and convergence speed, were simulated. The DSP transmitter and receiver were implemented with Spectrum TMS320C25 system boards.

Several important results are obtained in this thesis. First, the adjacent-channel interference power at the postdistortion receiver is analytically found to be a quadratic function of the amplifier coefficients as well as the postdistorter coefficients. This result is verified both through simulation and with the implemented system. Second, two different adaptation methods for postdistorter coefficients are presented. The first method is based on measuring the adjacent channel emissions in the bandwidth of the desired channel and then generating appropriate compensation signals. This approach, referred as the *power-based* method, requires idling of the desired (or center) channel while the receiver is adapting its postdistorters. The second method presents a different approach to adapt the postdistorters without the requirement of idling the center channel. The second adaptation method uses the variance of the received samples as an indication of adjacent-channel interference power, and hence is named the *variance-base* method. Finally, the simulation and measured results are given to demonstrate the performance of the adaptive postdistortion receiver.

This thesis is organized as follows. Chapter 2 describes the system overview and provides relevant background on bandpass signals, nonlinearities of power amplifiers, and the postdistorter characteristics. Chapter 3 presents the analysis for a simplified postdistortion system to determine the relationship between the postdistorter coefficients

and adjacent channel power. Chapter 4 discusses adaptation methods to optimize the postdistorter coefficients for slow drifts in power amplifier's characteristics. Chapters 5 and 6 present simulation models and results, respectively. Chapter 7 then gives details of the hardware implementation and results for the postdistortion system.

2 BACKGROUND

This chapter presents relevant background for the work on postdistortion system. Section 2.1 presents the overview of the postdistortion system. Section 2.2 reviews bandpass signals and a representation of multi-channel transmission. Section 2.3 describes the power amplifier nonlinearities, and Section 2.4 presents the characteristics of the postdistorter.

2.1 Overview of Postdistortion System

The purpose of the postdistortion technique is to reduce the interference in a channel which is caused by out-of-band emissions of the adjacent channels. The basic idea of the postdistortion technique is to compensate for the power amplifier's AM-AM and AM-PM nonlinearities [7] at the receiver. The postdistorter generates a nonlinear distortion signal based on the envelope of the received signal in such a way as to cancel the 3rd and 5th order IM products of the amplified signal. These IM products are the primary concerns of the postdistortion technique because they are within the bandwidth of the desired channel and cannot be filtered out completely by conventional filtering techniques. Upon combining the amplified and postdistorted signals, the IM products of the resulting signal should be drastically reduced. Figure 2.1 shows the block diagram of an adaptive postdistortion system.

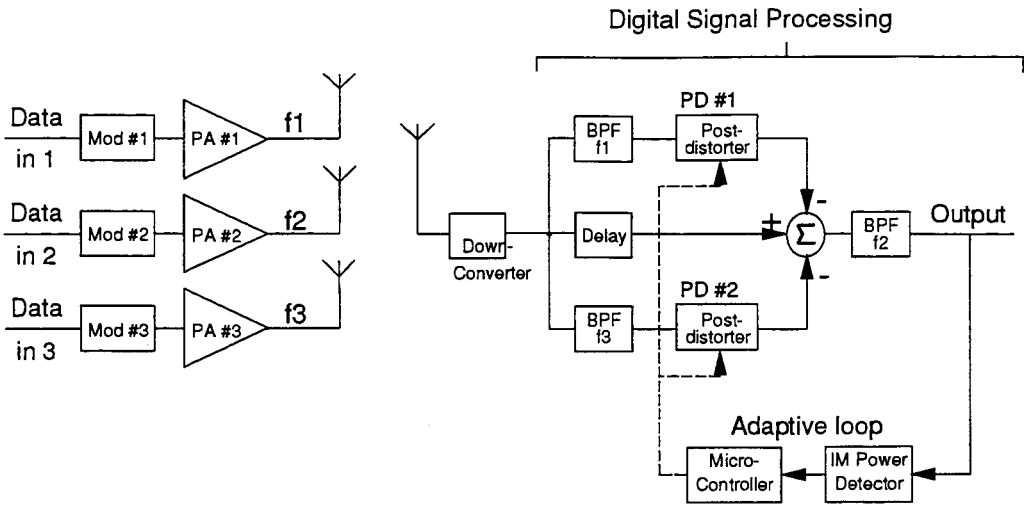

Figure 2.1 Block diagram of an adaptive postdistortion system

As shown in Figure 2.1, the modulated signals with adjacent carrier frequencies $f1$, $f2$ and $f3$ are amplified before they are fed to their respective transmitting antennas. Due to amplifier nonlinearities, out-of-band power from the adjacent channels, 1 and 3, will spill over into the desired channel, 2. This effect is undesirable because detection of channel 2's information will be very difficult if these IM powers are comparable to channel 2's power. The postdistortion technique solves this problem by generating IM products with equal amplitudes but opposite phases of those produced by the respective amplifiers. In particular, the bandpass filter BPF-f1 passes channel 1's information through to the postdistorter PD #1 which then generates the above mentioned IM products. Similarly, BPF-f3 passes channel 3's information to PD #2. A delay block is needed in the middle branch to equalize for the time delay in BPF-f1 and BPF-f3. The delayed and postdistorted signals are combined and then passed to BPF-f2. The output signal is now channel 2's information, free of spill-over interference. This signal is then fed to a demodulator.

The operating conditions of transmitters will gradually change with time due to component aging, temperature, etc.. These changes will affect the postdistorter performance. Hence an adaptive control is desired to optimize the system performance. The adaptive loop is comprised of an IM power detector and a micro-controller. The basic idea of the adaptive control is that while only channels 1 and 3 are transmitting, the micro-controller varies the postdistorter coefficients for minimum IM power in channel 2. In particular, while transmitter 2 is idle, the IM power detector samples the BPF-f2 output for spill-over power from channels 1 and 3. This information is then fed to the micro-controller which in turn adjusts the postdistorter coefficients based on the level of detected IM power.

2.2 Bandpass Signals

A real-valued bandpass signal can be represented by

$$x(t) = Re\{\tilde{x}(t)\} \tag{2.1}$$

where ω_c is the carrier frequency and $\tilde{x}(t)$ is the analytic signal associated with $x(t)$. This analytic signal is a complex-valued signal and represented by

$$\tilde{x}(t) = s(t)e^{j\omega_c t} \tag{2.2}$$

where $s(t)$ is the equivalent baseband signal of $x(t)$ with a bandwidth $B < \omega_c$.

In mobile communications, several channels are employed simultaneously to increase the number of users. Hence a representation of a multi-channel transmission is required. For convenience, analytic signals will be used in the representation of multi-channel transmission. Consider three analytic bandpass signals with carrier frequencies of ω_{c1}, ω_{c2} and ω_{c3} and their corresponding baseband signals of $s_1(t)$, $s_2(t)$ and $s_3(t)$, respectively.

$$\tilde{x}(t) = s_1(t)e^{j\omega_{c1}t} + s_2(t)e^{j\omega_{c2}t} + s_3(t)e^{j\omega_{c3}t} \tag{2.3}$$

Let

$$\Delta\omega_1 = \omega_{c1} - \omega_{c2} \tag{2.4}$$

$$\Delta\omega_3 = \omega_{c3} - \omega_{c2} \tag{2.5}$$

Then (2.3) can be rewritten as

$$\tilde{x}(t) = e^{j\omega_{c2}t} s_{eq}(t) \tag{2.6}$$

where $s_{eq}(t)$ is the equivalent baseband signal

$$s_{eq}(t) = s_1(t)e^{j\Delta\omega_1 t} + s_2(t) + s_3(t)e^{j\Delta\omega_3 t} \tag{2.7}$$

For mobile data communications, the carrier frequencies are equally spaced. Suppose that $\omega_{c1} < \omega_{c2} < \omega_{c3}$ and let $\Delta\omega = |\omega_{c1} - \omega_{c2}| = |\omega_{c3} - \omega_{c2}|$, then

$$\Delta\omega_1 = \omega_{c1} - \omega_{c2} = -\Delta\omega \tag{2.8}$$

$$\Delta\omega_3 = \omega_{c3} - \omega_{c2} = \Delta\omega \tag{2.9}$$

$$s_{eq}(t) = s_1(t)e^{-j\Delta\omega t} + s_2(t) + s_3(t)e^{j\Delta\omega t} \tag{2.10}$$

Therefore, the sum of multiple bandpass signals can be represented as an equivalent single bandpass signal whose baseband signal is the sum of their frequency-shifted baseband versions. Hence, to simulate multiple bandpass signals, one needs only to simulate their equivalent baseband signals according to (2.10).

2.3 Power Amplifier

A power amplifier is usually modelled as a *memoryless* system. A system is said memoryless if its output depends on its present input only, not its previous inputs. The input-output relationship of a nonlinear amplifier can be then represented by

$$V_a = V_m G(|x_m|) \tag{2.11}$$

where $x_m = |V_m|^2$ is the squared envelope of the input signal V_m and G is the nonlinear gain function. This nonlinear function, obtained from the AM-AM and AM-PM characteristics, can be expressed as

$$G(x_m) = \mathrm{P}(x_m)e^{j\Theta(x_m)} \tag{2.12}$$

where P and Θ are, respectively, the AM-AM and AM-PM conversions of the gain function [10]. Now, it is convenient to rewrite (2.12) as

$$G(x_m) = G_1(x_m) + jG_2(x_m) \tag{2.13}$$

where $G_1 = \mathrm{P}(x_m)\cos(\Theta(x_m))$ (2.14a)

$$G_2 = \mathrm{P}(x_m)\sin(\Theta(x_m)) \tag{2.14b}$$

G_1 and G_2 are, respectively, the real-valued functions representing the *in-phase* and *quadrature* components of the complex-valued gain function G. Figure 2.2 shows a block diagram of the amplifier.

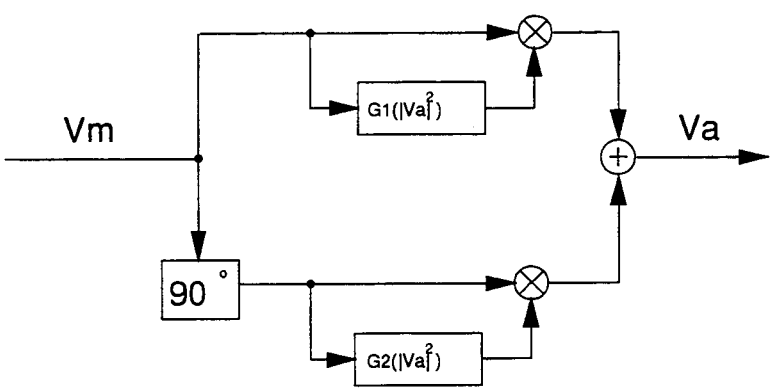

Figure 2.2 Block diagram of the power amplifier

Approximating G_1 and G_2 with power series yields [11]

$$G_1(x_m) = \beta_{11} + \beta_{31}x_m + \beta_{51}x_m^2 \tag{2.15}$$

$$G_2(x_m) = \beta_{12} + \beta_{32}x_m + \beta_{52}x_m^2 \tag{2.16}$$

where the motivation for the indexing scheme of the constants is given below.

Thus the gain function can be rewritten as

$$G(x_m) = \beta_1 + \beta_3 x_m + \beta_5 x_m^2 \tag{2.17}$$

where β's are the complex-valued amplifier coefficients and defined as

$$\beta_1 = \beta_{11} + j\beta_{12} \tag{2.18a}$$

$$\beta_3 = \beta_{31} + j\beta_{32} \tag{2.18b}$$

$$\beta_5 = \beta_{51} + j\beta_{52} \tag{2.18c}$$

Substituting (2.17) into (2.11) gives

$$V_a = V_m(\beta_1 + \beta_3 |V_m|^2 + \beta_5 |V_m|^4) \tag{2.19}$$

Upon expansion of (2.19), the first term $\beta_1 V_m$ is a linear term; the higher order terms $\beta_3 V_m |V_m|^2$ and $\beta_5 V_m |V_m|^4$ are nonlinear terms which cause the 3rd and 5th order IM products, respectively, in an adjacent channel. In other words, these nonlinear terms cause spreading of the output spectrum.

2.4 Postdistorter

The basic function of the postdistorter is to generate the same IM products produced by the power amplifier. Therefore, the postdistortion function is an approximation of the power amplifier's characteristics which are modelled as a memoryless nonlinearity [6]. The input-output relationship of the postdistorter is given by

$$V_d = V_a \cdot F(|V_a|^2) \tag{2.20}$$

where V_a is the input and F is the postdistorter function. Similar to the amplifier gain function presented in Section 2.3, the postdistortion function is represented by a complex polynomial

$$F(x_a) = \alpha_1 + \alpha_3 x_a^2 + \alpha_5 x_a^4 \tag{2.21}$$

where $x_a = |V_a|^2$ is the squared envelope of the amplified signal V_a and each postdistorter coefficient is a complex number. Let define the postdistorter coefficients as

$$\alpha_1 = \alpha_{11} + j\alpha_{12} \tag{2.22a}$$

$$\alpha_3 = \alpha_{31} + j\alpha_{32} \tag{2.22b}$$

$$\alpha_5 = \alpha_{51} + j\alpha_{52} \tag{2.22c}$$

Hence, the postdistortion function can be written as

$$F(x_a) = F_1(x_a) + jF_2(x_a) \tag{2.23}$$

where $$F_1(x_a) = \alpha_{11} + \alpha_{31}x_a + \alpha_{51}x_a^2 \tag{2.24a}$$

$$F_2(x_a) = \alpha_{12} + \alpha_{32}x_a + \alpha_{52}x_a^2 \tag{2.24b}$$

In these equations, the α-coefficients are constants which depend on the PA nonlinearity. Section 3.2 shows how to select these coefficients. F_1 and F_2 are the real-valued functions representing the in-phase and quadrature components, respectively, of the complex-valued postdistorted function F. Figure 2.3 shows a block diagram of the postdistorter.

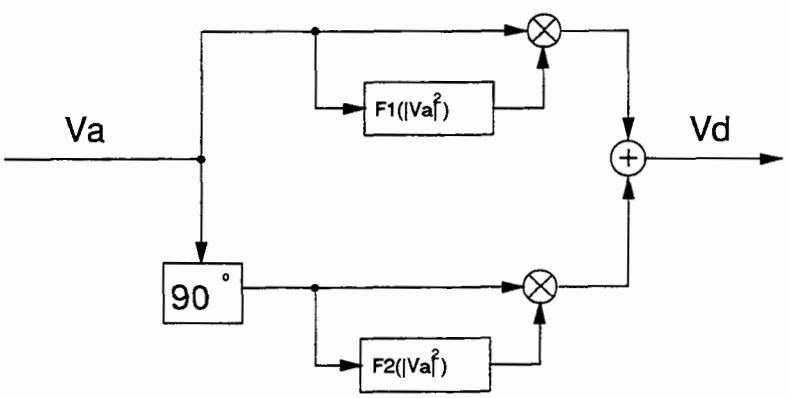

Figure 2.3 Block diagram of the postdistorter

3 ANALYSIS

This chapter describes the analysis model and presents the out-of-band emission analysis for a simplified postdistortion system using zero-mean Gaussian inputs. The simplified system considers only one adjacent channel and evaluates the IM power in that channel after postdistortion. Hence this analysis assumes that only one adjacent, say channel 1, is active while the center channel and the other adjacent channel, channels 2 and 3, are off.

3.1 Analysis Model

Figure 3 shows the block diagram of a simplified postdistortion system consisting of a power amplifier, two bandpass filters, a postdistorter, and a delay line. All the bandpass filters are assumed to be ideal to simplify the analysis. The BPF #1 is tuned to channel 1, and its purpose is to extract the linear term generated by the power amplifier. Note that the extracted signal also contains contributions from the nonlinear terms. Because the nonlinear terms are generally much smaller than the linear term, their effects will be ignored in the analysis. The delay line in the lower branch is used to compensate for time delay in BPF #1. After the postdistorted signal is subtracted from the delayed signal, the resulting signal is fed to BPF #2 which is tuned to channel 2. The function of this filter is to approximate a distortion filter. Since the fundamental components of the resulting signal is outside the bandwidth of BPF #2, the filter output will equivalently contain the distortion signal only. Compared with the block diagram shown in Figure 2.1, this simplified postdistortion system is only a portion (upper branch or lower branch) of the complete system without the adaptive loop. In other words, the complete system

consists of two simplified systems which both minimize the IM products of the corresponding adjacent channel. Therefore, it is sufficient to analyze only the simplified system.

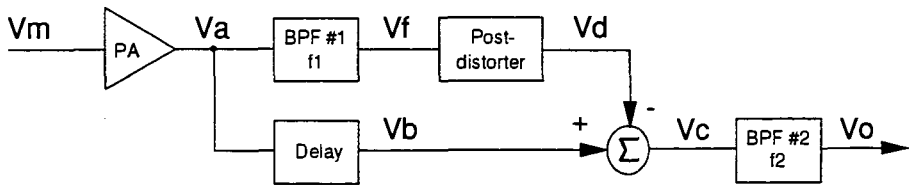

Figure 3 Block diagram of a simplified postdistortion system

3.2 System Analysis

Assume that the real-valued input signal is a wide-sense stationary (WSS) process. Furthermore, for analysis purposes, assume that the input is a narrowband bandpass Gaussian input with zero mean [10]

$$\tilde{V}_m(t) = Re\left\{ V_m(t) e^{j2\pi f_1 t} \right\} \tag{3.1}$$

where $V_m(t)$ is its baseband complex envelope and f_1 is the channel 1's carrier frequency. For convenience, most of the analysis will be carried out in the complex domain.

Due to AM-AM and AM-PM nonlinearities of the power amplifier, the transmitter output signal is given by

$$\begin{aligned} V_a(t) &= V_m(t) \cdot G(|V_m(t)|^2) \\ &= V_m(t)[\beta_1 + \beta_3 x_m(t) + \beta_5 x_m^2(t)] \end{aligned} \tag{3.2}$$

where $x_m(t) = |V_m(t)|^2$ and G is the amplifier gain function described in Section 2.3.

The autocorrelation function of the complex envelope $V_m(t)$ is defined as

$$R_a(\tau) = \frac{1}{2} E\{V_a(t) V_a^*(t-\tau)\} \tag{3.3}$$

The autocorrelation function can be evaluated using the formula for mixed moments of zero-mean jointly Gaussian random variables [9]. The resulting autocorrelation function of the amplifier complex envelope is

$$R_a(\tau) = P_1 R_m(\tau) + P_3 R_m^*(\tau) R_m^2(\tau) + P_5 R_m^{*2}(\tau) R_m^3(\tau) \tag{3.4}$$

where $$P_1 = |\beta_1 + 4\beta_3 R_m(0) + 24\beta_5 R_m^2(0)|^2 \tag{3.5a}$$

$$P_3 = 8|\beta_3 + 12\beta_5 R_m(0)|^2 \tag{3.5b}$$

$$P_5 = 192|\beta_5|^2 \tag{3.5c}$$

Taking the Fourier transform of (3.4) gives the power spectral density (PSD) of the amplified signal $V_a(t)$ as

$$S_a(f) = P_1 S_m(f) + P_3 S_{m3}(f) + P_5 S_{m5}(f) \tag{3.6}$$

where $$S_m(f) = \mathcal{F}\{R_m(\tau)\} \tag{3.7a}$$

$$S_{m3}(f) = S_m(-f) \otimes S_m(f) \otimes S_m(f) \tag{3.7b}$$

$$S_{m5}(f) = S_m(-f) \otimes S_m(-f) \otimes S_m(f) \otimes S_m(f) \otimes S_m(f) \tag{3.7c}$$

and $\otimes$ represents convolution.

Here $P_1 S_m(f)$ is the spectrum density of the fundamental components, whereas $P_3 S_{m3}(f)$ and $P_5 S_{m5}(f)$ are the spectra of the 3rd and 5th order IM products, respectively. As assumed above, the BPF #1 selects only the fundamental components produced by PA; hence the PSD function of the filter output is

$$S_f(f) = P_1 S_m(f) \tag{3.8}$$

Taking the inverse Fourier transform of (3.8) gives the autocorrelation function of the filter output

$$R_f(\tau) = P_1 R_m(\tau) \tag{3.9}$$

And subsequently, the filter output is written as

$$V_f(t) = \sqrt{P_1}\, V_m(t) \tag{3.10}$$

The postdistorter output is given by

$$\begin{aligned} V_d(t) &= V_f(t) \cdot F(|V_f(t)|^2) \\ &= V_f(t)[\alpha_1 + \alpha_3 x_f(t) + \alpha_5 x_f^2(t)] \end{aligned} \tag{3.11}$$

where $x_f(t) = |V_f(t)|^2 = P_1 x_m(t)$ and F is the postdistortion function described in Section 2.4.

Hence the postdistorter output is

$$V_d(t) = V_m(t)[\alpha_1 P_1^{1/2} + \alpha_3 P_1^{3/2} x_m(t) + \alpha_5 P_1^{5/2} x_m^2(t)] \tag{3.12}$$

Assuming that the delay line is ideal, its sole purpose is to compensate for delay time in BPF #1. Hence the time delay effects of the delay line and BPF #1 will not be considered. The delayed signal is then

$$V_b(t) = V_a(t) \tag{3.13}$$

The input signal to BPF #2 is

$$V_c(t) = V_a(t) - V_d(t) \tag{3.14}$$

Substituting (3.2) and (3.12) into (3.14) yields

$$V_c(t) = V_m(t)[\gamma_1 + \gamma_3 x_m(t) + \gamma_5 x_m^2(t)] \tag{3.15}$$

where

$$\gamma_1 = \beta_1 - \alpha_1 P_1^{1/2} \tag{3.16a}$$

$$\gamma_3 = \beta_3 - \alpha_3 P_1^{3/2} \tag{3.16b}$$

$$\gamma_5 = \beta_5 - \alpha_5 P_1^{5/2} \tag{3.16c}$$

Since (3.15) is similar to (3.2), the autocorrelation and PSD functions of $V_c(t)$ have the following forms

$$R_c(\tau) = K_1 R_m(\tau) + K_3 R_m^*(\tau) R_m^2(\tau) + K_5 R_m^{*2}(\tau) R_m^3(\tau) \tag{3.17}$$

$$S_c(f) = K_1 S_m(f) + K_3 S_{m3}(f) + K_5 S_{m5}(f) \tag{3.18}$$

where

$$K_1 = |\gamma_1 + 4\gamma_3 R_m(0) + 24\gamma_5^2 R_m^2(0)|^2 \tag{3.19a}$$

$$K_3 = 8|\gamma_3 + 12\gamma_5 R_m(0)|^2 \tag{3.19b}$$

$$K_5 = 192|\gamma_5|^2 \tag{3.19c}$$

From (3.18), $K_1 S_m(f)$ is the spectrum density of the fundamental components of $V_c(t)$, whereas $K_3 S_{m3}(f)$ and $K_5 S_{m5}(f)$ are the spectra of the 3rd and 5th order IM products of $V_c(t)$, respectively.

Now, the bandpass representation of $V_c(t)$ is

$$\tilde{V}_c(t) = Re\left\{ V_c(t) e^{j\omega_1 t} \right\} \tag{3.20}$$

The relationship between the autocorrelation functions of the bandpass and baseband signals is [10]:

$$\begin{aligned} \tilde{R}_c(\tau) &= Re\left\{ R_c(\tau) e^{j2\pi f_1 \tau} \right\} \\ &= \frac{1}{2}\left[R_c(\tau) e^{j2\pi f_1 \tau} + R_c^*(\tau) e^{-j2\pi f_1 \tau} \right] \end{aligned} \tag{3.21}$$

The PSD function of the bandpass signal $\tilde{V}_c(t)$ is therefore

$$\tilde{S}_c(f) = \frac{1}{2}[S_c(f - f_1) + S_c(-f - f_1)] \tag{3.22}$$

Note that $\tilde{S}_c(f)$ is a real and even function.

As assumed above, the input $\tilde{V}_m(t)$ is a narrowband bandpass Gaussian process; hence its PSD is confined within the bandwidth of channel 1. Consequently, BPF #2 will filter out the fundamental components of $\tilde{V}_c(t)$ but pass through a portion of 3rd and 5th order IM products. In other words, BPF #2 output is a measure of the out-of-band emission of channel 1 injected into channel 2. The PSD function of the bandpass output signal is

$$\tilde{S}_o(f)=\begin{cases}\tilde{S}_c(f), & f_2-\dfrac{\Delta f}{2}\le|f|\le f_2+\dfrac{\Delta f}{2};\\ 0, & \text{otherwise}\end{cases} \tag{3.23}$$

$$\tilde{S}_o(f)=\begin{cases}\dfrac{1}{2}K_3[S_{m3}(f-f_1)+S_{m3}(-f-f_1)]+\dfrac{1}{2}K_5[S_{m5}(f-f_1)+S_{m5}(-f-f_1)], & f_2-\dfrac{\Delta f}{2}<|f|<f_2+\dfrac{\Delta f}{2};\\ 0, & \text{otherwise}\end{cases}$$

where $f_2=f_1+\Delta f$.

Note that $\tilde{S}_o(f)$ is also real and even. Integrating PSD $\tilde{S}_o(f)$ over channel 2's bandwidth gives the out-of-band emission power. Now by dividing the out-of-band power by the bandwidth, one can obtain the average of output IM power, or simply average IM power, P_{IM}.

$$\begin{aligned}P_{IM}&=\frac{1}{\Delta f}\left[\int_{f_2-\frac{\Delta f}{2}}^{f_2+\frac{\Delta f}{2}}\tilde{S}_o(f)df+\int_{-f_2-\frac{\Delta f}{2}}^{-f_2+\frac{\Delta f}{2}}\tilde{S}_o(f)df\right]\\&=\frac{2}{\Delta f}\int_{f_2-\frac{\Delta f}{2}}^{f_2+\frac{\Delta f}{2}}\tilde{S}_o(f)df\\&=K_3P_{IM3}+K_5P_{IM5}\end{aligned} \tag{3.24}$$

where

$$P_{IM3} = \frac{2}{\Delta f} \int_{\frac{\Delta f}{2}}^{\frac{3\Delta f}{2}} S_{m3}(f) df \tag{3.25a}$$

$$P_{IM5} = \frac{2}{\Delta f} \int_{\frac{\Delta f}{2}}^{\frac{3\Delta f}{2}} S_{m5}(f) df \tag{3.25b}$$

Observing from (3.24), the average IM power depends on P_{IM3} and P_{IM5} which both are nonnegative. Therefore, to minimize the average IM power, it requires that K_3 and K_5 equal zero. Solving for α's, one obtains the approximate postdistorter coefficients as

$$\hat{\alpha}_1 = 1 \tag{3.26a}$$

$$\hat{\alpha}_3 = \frac{\beta_3}{P_1^{3/2}} \tag{3.26b}$$

$$\hat{\alpha}_5 = \frac{\beta_5}{P_1^{5/2}} \tag{3.26c}$$

Because the amplifier coefficient β_1 is generally very close to unity, setting the postdistorter coefficient $\hat{\alpha}_1$ to unity will partially optimize that coefficient. Consequently, the specifications for BPF-f2 in Figure 2.1 can then be relaxed. In other words, when α_1 is not optimized, it is more difficult for BPF-f2 to filter out the fundamental components of channels 1 and 3 because their powers are comparable to the inband power of channel 2.

For convenience, define

$$\alpha_3 = \hat{\alpha}_3 + \Delta\alpha_3 \tag{3.27a}$$

$$\alpha_5 = \hat{\alpha}_5 + \Delta\alpha_5 \tag{3.27b}$$

where $\Delta\alpha_3$ and $\Delta\alpha_5$ are the deviations of α_3 and α_5, respectively, from their optimal coefficients. Hence (3.24) can be rewritten as

$$\begin{aligned} P_{IM} &= 8P_1^3|\Delta\alpha_3 + 12P_1R_m^2(0)\Delta\alpha_5|^2 P_{IM3} + 192P_1^5|\Delta\alpha_5|^2 P_{IM5} \\ &= 8P_1^3 P_{IM3}\left[|\Delta\alpha_3|^2 + 24P_1R_m^2(0)Re\{\Delta\alpha_3\Delta\alpha_5^*\} + 24P_1^2\left(6R_m^4(0) + \frac{P_{IM5}}{P_{IM3}}\right)|\Delta\alpha_5|^2\right] \end{aligned} \tag{3.28}$$

It is evident that the average IM power is a quadratic function in terms of the postdistorter coefficients. Therefore, $\hat{\alpha}_3, \hat{\alpha}_5$ must be the global minimum due to the quadratic nature of P_{IM}. Note that each coefficient in (3.28) is a complex variable, hence the average IM power P_{IM} is a 4-dimensional function of real variables α_{31}, α_{32}, α_{51} and α_{52}. To visualize the behaviour of this function about its minimum, one can examine its 'shape' in 2-dimension at time by setting, for instance, $\alpha_5 = \hat{\alpha}_5$. That is $\Delta\alpha_5 = 0$; hence the IM power in α_3 plane is

$$\begin{aligned} P_{IM} &= 8P_1^3 P_{IM3}|\Delta\alpha_3|^2 \\ &= 8P_1^3 P_{IM3}(\Delta\alpha_{31}^2 + \Delta\alpha_{32}^2) \end{aligned} \tag{3.29}$$

It is evident that this function is a paraboloid with its global minimum at $\alpha_3 = \hat{\alpha}_3$. In other words, as the coefficient α_3 deviates from its optimal value, the IM power increases as a square function of the deviation, given that $\alpha_5 = \hat{\alpha}_5$. Similarly, by setting $\alpha_3 = \hat{\alpha}_3$, (3.28) becomes

$$\begin{aligned} P_{IM} &= 192P_1^5[6R_m^4(0)P_{IM3} + P_{IM5}]|\Delta\alpha_5|^2 \\ &= 192P_1^5[6R_m^4(0)P_{IM3} + P_{IM5}](\Delta\alpha_{51}^2 + \Delta\alpha_{52}^2) \end{aligned} \tag{3.30}$$

Equation (3.30) evidently shows the quadratic dependence of the output IM power in the α_5 plane.

In summary, two main conclusions can be drawn based on the IM power function:

- The average output IM power has a 'parabolic' shape (i.e., quadratic functions of α_3's and α_5's); hence there exists a global minimum which can be found by adaptation algorithms.
- This IM power depends on both α_3's and α_5's, and especially the cross term of these coefficients in (3.28). In other words, the interaction between these coefficients cannot be decoupled. Therefore, it is necessary to jointly optimize the α_3's and the α_5's.

Initially, the power amplifier coefficients can be obtained from the AM-AM and AM-PM measurements of the amplifier by using the least-square fitting method. However, the least-square method does not always guarantee the optimal coefficients. Because if one tried to fit the amplifier gain function described in (2.3) to most of the measured data points, one would approximate the linear region of the amplifier's characteristics. Therefore, this approach does not accurately approximate the nonlinear region which is responsible for IM products. Moreover, the analysis results are based on the first approximation of the bandpass filter BPF #1 and the distortion filter BPF #2. To take into account the second order effects of these filters, optimization is a necessity. Furthermore, the above analysis only considers the static case where the amplifier's characteristics are assumed to be constant over time. This assumption works fairly well but does not truly reflect the real case. In order to minimize the IM products from adjacent channels and to adapt to variations in amplifiers' characteristics, adaptation methods should be utilized.

4 ADAPTATION METHODS

The analysis in Chapter 3 shows that the out-of-band power is a quadratic function of the postdistorter coefficients. Hence there exists a global minimum which can be found by various optimization algorithms. Hooke and Jeeves' algorithm [8,11], a direct search method, is used to adapt the postdistorter coefficients because of its simplicity and robustness. After selecting an adaptation algorithm, the most important task is setting up the *objective function.* In particular, the objective function of the postdistortion technique is to minimize the adjacent-channel power interference. This chapter describes two methods from two different perspectives to setup the objective function. The first method which is stemmed from the frequency-domain viewpoint, directly uses the measured IM power as the objective function. This is the traditional method used in predistortion techniques [4-7] where the amplifier nonlinearities are corrected at the transmitter. The second method which has originated from the time-domain perspective, employes the variance of the sampled signal as the objective function.

4.1 IM Power-Based Method

Section 3.2 shows that the average IM power is a quadratic function of the postdistorter coefficients. To minimize this IM power, it is natural to use the measured IM power as the objective function. Figure 4.1 shows a typical power spectrum at the BPF #2 input of the system shown in Figure 2.1. In this measurement, channels 1 and 2 are idle, only channel 3 is transmitting. The IM power is calculated as the average power, in the frequencies ranging from $f_L = -\frac{\Delta f}{2}$ to $f_H = \frac{\Delta f}{2}$, with respect to a *reference level.* This frequency range is allocated to channel 2, and is defined as the *noise window.* The reference level is selected at -65 dBm.

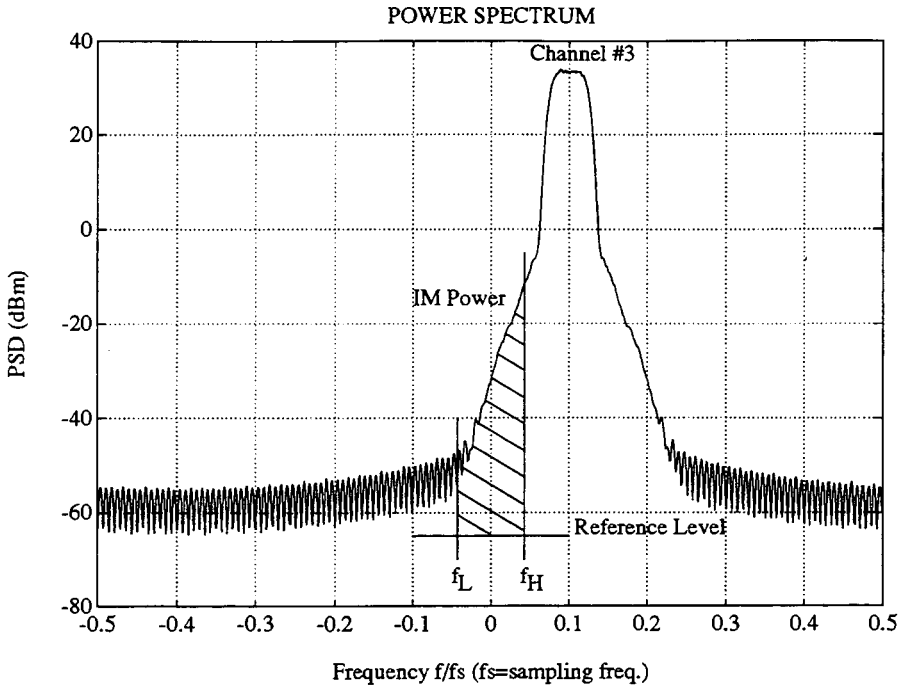

Figure 4.1 Power spectrum showing a setup for IM power calculation

The measured power is the adjacent channel power in the bandwidth of the desired channel, channel 2. Using this power as a feedback, the postdistorter coefficients are iteratively adjusted according to the adaptation algorithm. As mentioned in the introduction, slow variations of the transmitter amplifier do not require frequent adaptation of the postdistorter. This works effectively in Time Division Multiple Access (TDMA) applications. While the transmitter #2 is waiting (i.e., idle) for its turn to transmit, the postdistorters can adapt to adjacent channels' amplifiers to establish an acceptable noise floor. When channel 2 is ready to transmit, it then has an optimal SNR.

However, the setup shown in Figure 2.1 has a drawback that channel 2 is required to be idle during postdistorter adaptation. Switching of adjacent channels to different portable transmitter amplifiers may degrade the performance of the postdistorters. Therefore adaptation of the postdistorters in the presence of channel 2 is desirable.

4.2 Variance-Based Method

This section presents a modification that can adapt the postdistorter coefficients while channel 2 is also transmitting. The objective function is to minimize the variance of the sampled signal after postdistortion. Figure 4.2 shows the block diagram of the modified postdistortion receiver.

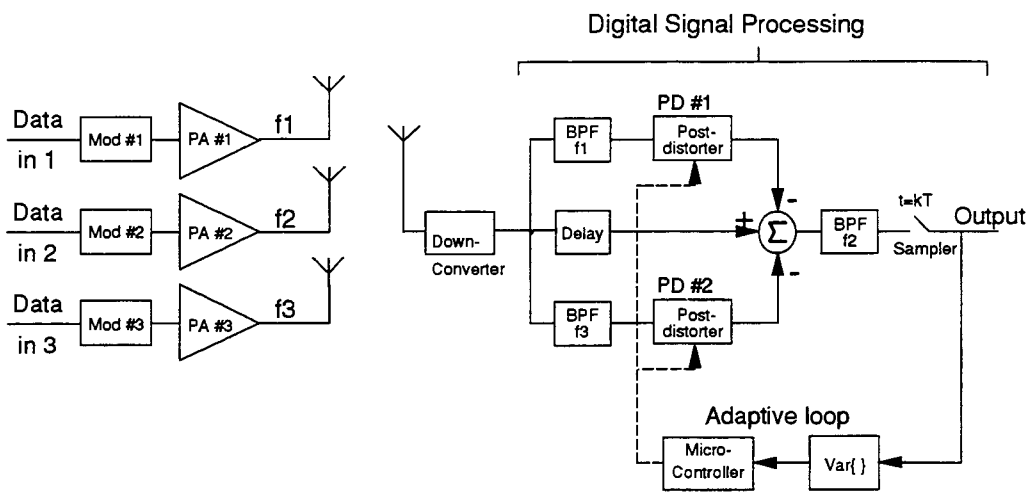

Figure 4.2 Block diagram of the modified postdistortion receiver

Note that in this setup, the sampler and variance blocks replace the IM power detector block in Figure 2.1. The I and Q outputs of BPF-f2 are sampled at the symbol rate. For OQPSK signal, the Q signal is sampled with a delay of a half symbol-time with respect to the I signal. Plotting the I and Q samples in I-Q axes gives the constellation depicted in Figure 4.3.

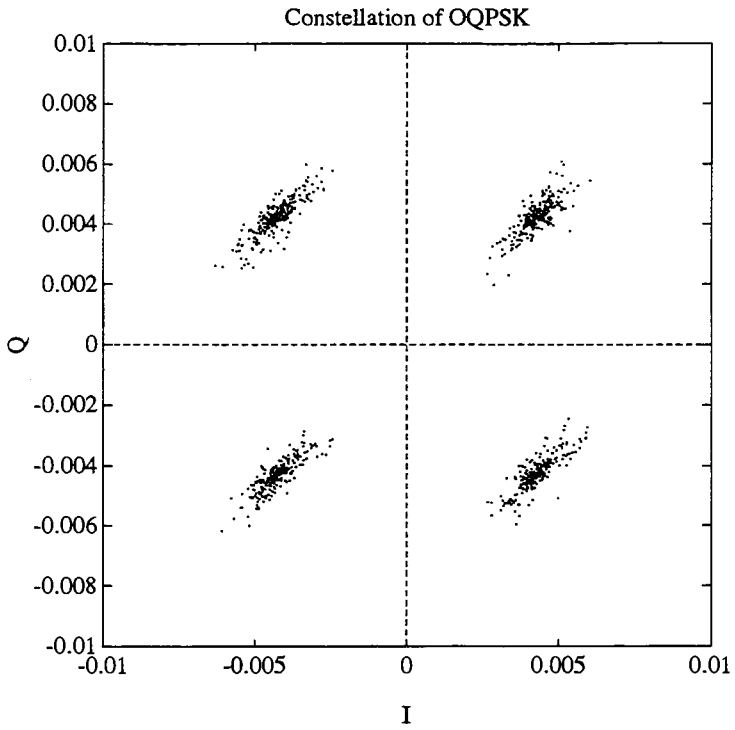

Figure 4.3 Constellation of a received signal

Figure 4.3 shows four distinct clusters of points which ideally should be confined to four distinct points only. As shown by the simulation results, the IM power of the adjacent channels and the equivalent noise power in channel 2 (due to its own amplifier nonlinearities) cause spreading of the constellation. Therefore the constellation variance is a good indication of adjacent channel power. The objective function is then defined as

$$f(\alpha) = \frac{1}{4}\sum_{i=1}^{4} var\{x^{(i)}\} \tag{4.1}$$

where $x^{(i)}$ is a point (or sample) in the ith quadrant of the constellation and the quantity in the summation is the variance of samples in the ith quadrant. Similar to the power-based method, it can be shown that the objective function of the variance-based method is a quadratic function of the postdistorter coefficients α's. The variance in each quadrant is estimated as

$$var\{x^{(i)}\} = \frac{1}{N_i}\sum_{k=1}^{N_i} |x_k^{(i)} - m_x^{(i)}|^2 \tag{4.2}$$

where $x_k^{(i)}$ and N_i are, respectively, the kth sample and the number of samples in the ith quadrant and $m_x^{(i)}$ is the mean of the samples in the ith quadrant and is defined as

$$m_x^{(i)} = \frac{1}{N_i}\sum_{k=1}^{N_i} x_k^{(i)} \tag{4.3}$$

The effective signal-to-noise ratio can be then expressed as

$$SNR = \frac{|m_x|^2}{\sigma_x^2} \tag{4.4}$$

where m_x is the average sample mean and σ_x^2 is the average sample variance which is $f(\alpha)$. From (4.1) and (4.4), minimizing the constellation variance implies maximizing the SNR.

In contrast to the IM power-based method, this method does not require idling the desired channel while the postdistorters are adapted; thereby making the variance-based method more convenient to use. Since switching of adjacent channels can be frequent and unpredictable, continually monitoring the adjacent channel power can therefore keep the postdistorters optimal.

Note that the variance-based method works effectively with the additive Gaussian noise channel. In fading channel conditions, considered in Section 6.3.3, the phase

information of a received signal will be shifted randomly; hence making detection impossible. There are a few available solutions in the literature such as using pilot symbol assisted technique for phase correction [20], or using DPSK signals [10] or including a phase tracking block.

5 SIMULATION MODELS

This chapter presents simulation models for the transmitter and receiver. Note that all the simulations were performed in baseband; therefore, all the frequencies are relative to the carrier frequency of the center channel.

5.1 Transmitter Model

The transmitter module can simulate three independent channels, one desired channel, 2, and two adjacent channels, 1 and 3. Figure 5.1 shows the transmitter model which consists of 3 modulators, 3 power amplifiers, 2 frequency converters and a summer. For demonstration purposes, Offset Quadrature Phase Shift Keying (OQPSK) modulators and class AB amplifiers were used. All operated in baseband except the two frequency converters. In order to simulate the system in baseband, the whole system was down converted by an amount equal to the carrier frequency of the center channel ω_{c2} (Section 2.2). That is, channel 1 was down converted relative to the center carrier ω_{c2} by $-\Delta\omega$, whereas channel 3 was up converted by $\Delta\omega$ where $\Delta\omega$ is the channel bandwidth.

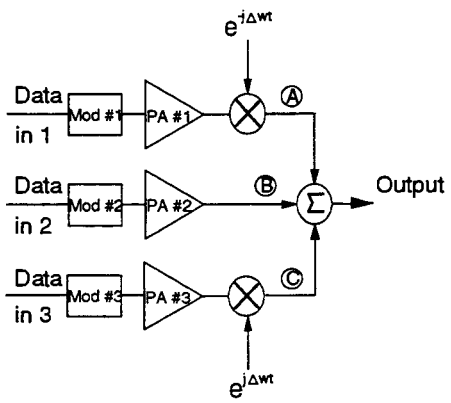

Figure 5.1 Transmitter model

5.1.1 Transmit Modem

Offset QPSK modulation was used in the simulation [12]. Offset QPSK is like QPSK, except that the quadrature component output is delayed by one-half a symbol-time. Mathematically, the offset QPSK output is expressed as

$$V_m(t) = \sum_{n=-\infty}^{\infty} \left(a_n g(t - nT) + j b_n g\left(t - nT - \frac{T}{2} \right) \right) \tag{5.1}$$

where T is the symbol period, $g(t)$ is the pulse shape, a_n's and b_n's are ± 1 depending on the input data bits. A raised-cosine pulse shape was used. This pulse shape is defined as

$$g(t) = \left\{ \frac{\sin(\pi t/T)}{\pi t/T} \right\} \left\{ \frac{\cos(\alpha \pi t/T)}{1 - (2\alpha t/T)^2} \right\} \tag{5.2}$$

where the roll-off factor α of 0.25 was used. The pulse was truncated to 7 symbols in length and sampled at 20 samples per symbol, and the resulting sequence was Kaiser windowed with Kaiser parameter of 6 [13]. The symbol rate of the system in simulation was 2,500 symbols per second; the sampling frequency and channel bandwidth were 50 kHz and 5 kHz, respectively.

5.1.2 Power Amplifier

The power amplifiers in simulation were based on the measured characteristics of a class AB, 5 Watt amplifier from 3dbm [14]. The measured AM-AM and AM-PM characteristics were converted to the in-phase and quadrature gain functions according to (2.13). These gain functions were then approximated and normalized to quintic polynomials

$$G_1(x) = 0.99344 + 0.12073x - 0.40774x^2 + 0.21695x^3 - 0.04888x^4 + 0.00409x^5 \tag{5.3a}$$

$$G_2(x) = -0.00057 + 0.02086x + 0.12611x^2 - 0.10851x^3 + 0.03363x^4 - 0.00367x^5 \tag{5.3b}$$

where $x = |v|^2$ is the squared envelope of the input voltage v. The normalized gain function is shown in Figure 5.2

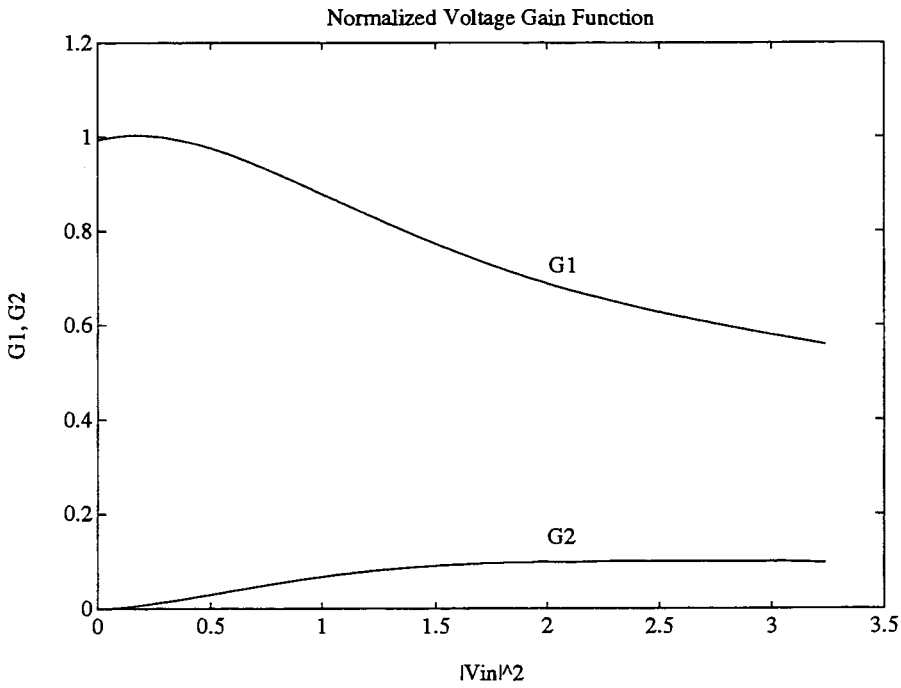

Figure 5.2 Complex gain of a class AB amplifier

The amplifier's operating point is controlled by scaling the input voltage. The Output power Back-Off (OBO) which measures how close to saturation the amplifier operating, is defined as

$$OBO = 10 \cdot \log_{10} \frac{P_{sat}}{P_{avg}} \tag{5.4}$$

where P_{sat} and P_{avg} are the saturated and average output powers, respectively.

5.2 Receiver Model

Figure 5.3 shows the receiver model. Because the postdistorters operate in baseband (Section 2.4), the inputs must be appropriately down/up converted before applying to the postdistorters. In particular, the postdistorter PD #1 minimizes the IM products produced by the amplifier PA #1 by generating the same IM products but opposite in phase. However, the received signal of channel 1 is already down converted by $\Delta\omega$, this signal must be up converted by the same amount before lowpass filtering to extract the channel 1's information. The filtered signal is fed to the postdistorter PD #1. The postdistorted signal is then down converted again before it is subtracted from the delayed composite signal. Similar actions happen in channel 3. The combined signal, at point B, consists of channel 2 and reduced IM signals of channels 1 and 3. This signal is finally lowpass filtered to recover channel 2's information.

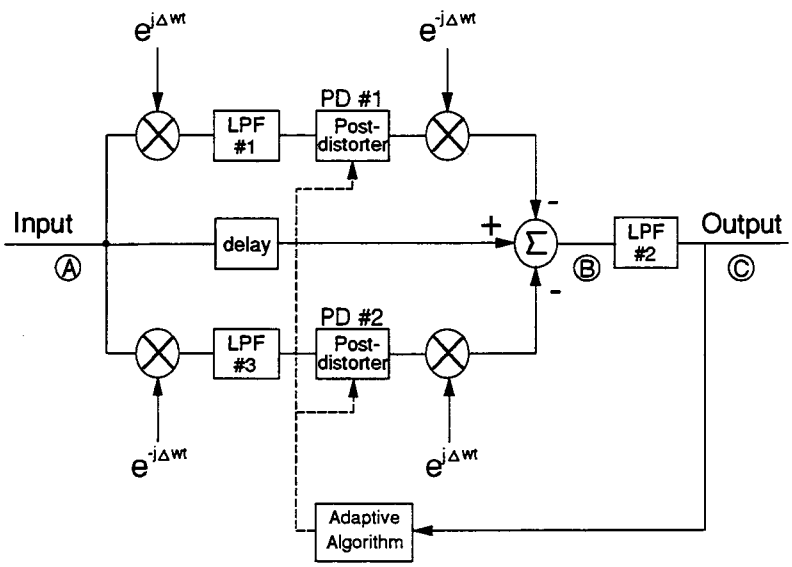

Figure 5.3 Receiver model

5.2.1 Lowpass Filter

All the lowpass filters are FIR filters and have the same characteristics. The cutoff frequency and transition band were, respectively, selected at 0.043 and 0.01 (f/f_s), where f_s is the sampling frequency. The filter provides 70 dB attenuation in the stopband. The cutoff frequency and transition band are equivalent to 2.15 kHz and 500 Hz, respectively, for a system with a symbol rate of 2500 symbols per second. Because of very narrow transition band and high attenuation in the stopband, the filter lengths are relative long, 367 taps. Figure 5.4 shows the frequency response of the filter.

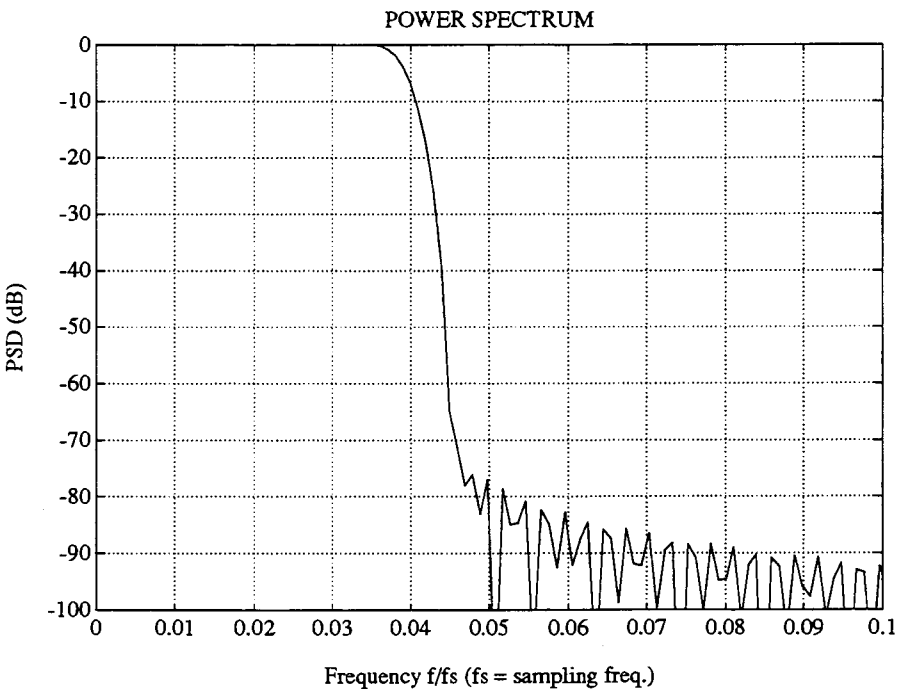

Figure 5.4 Lowpass filter frequency response

5.2.2 Postdistorter

The postdistorter is a quintic polynomial as presented in Section 2.4. The postdistorter function is given by

$$F(x_a) = \alpha_1 + \alpha_3 x_a + \alpha_5 x_a^2 \tag{5.4}$$

where x_a is the input power to the postdistorter. In the simulation, α_1 was initialized to unity to partially match with the amplifier (Section 4.2). The complex α_3 and α_5 coefficients were then adjusted by the adaptation algorithm presented in Chapter 4.

6 SIMULATION RESULTS

The simulation results are divided into three parts. Section 6.1 confirms the quadratic dependence of adjacent channel power on the postdistorter coefficients as derived in the analysis. Section 6.2 presents the adaptation results based on the IM power and variance methods. Section 6.3 presents the system performance, including SNR and convergence speed, and considers the system performance in fading channel conditions. Section 6.4 demonstrated the effect of the postdistortion technique on the mobile transmitter power efficiency and the spectral efficiency.

6.1 Quadratic Dependence of Adjacent Channel Power

This section demonstrates the quadratic function of adjacent channel power on the postdistorter coefficients. The simulation models shown in Figures 5.1 and 5.3 were used to measure the out-of-band power produced by a single adjacent channel, 1 or 3 only; for instance, channels 1 and 2 were off but channel 3 on. Figures 6.1 and 6.2 show the adjacent-channel power versus postdistorter coefficients where the power amplifier #3 operated at 2 dB OBO. In the simulation, 1000 symbols were used for each power measurement, and the coefficients not graphed were set to their optimal values.

The figures clearly show the predicted quadratic shape of adjacent channel power for all four postdistorter coefficients. Figure 6.2 shows that the adjacent channel power is more sensitive to mis-adjustment of the α_5 coefficient than that of the α_3 coefficient.

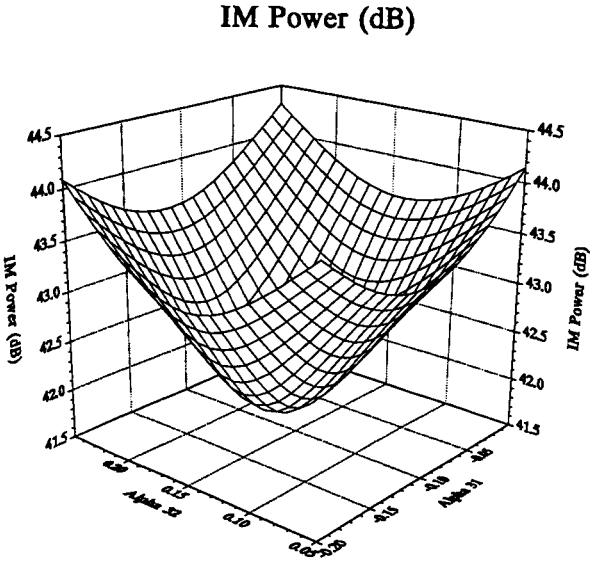

(a) Surface plot

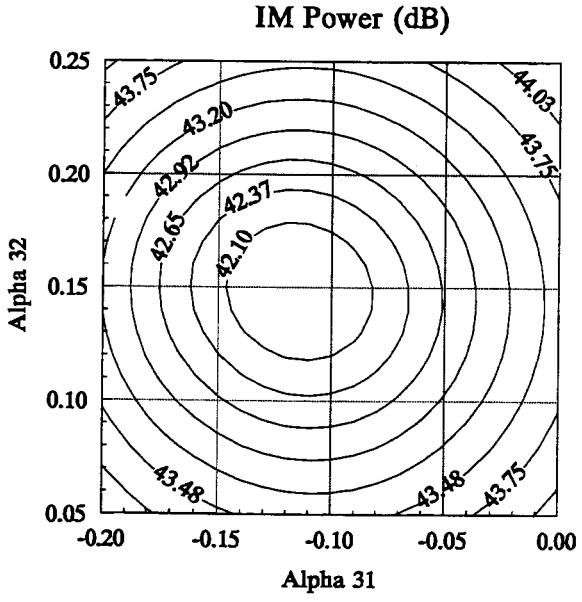

(b) Contour plot

Figure 6.1 Simulated adjacent-channel power versus α_3, OBO = 2 dB

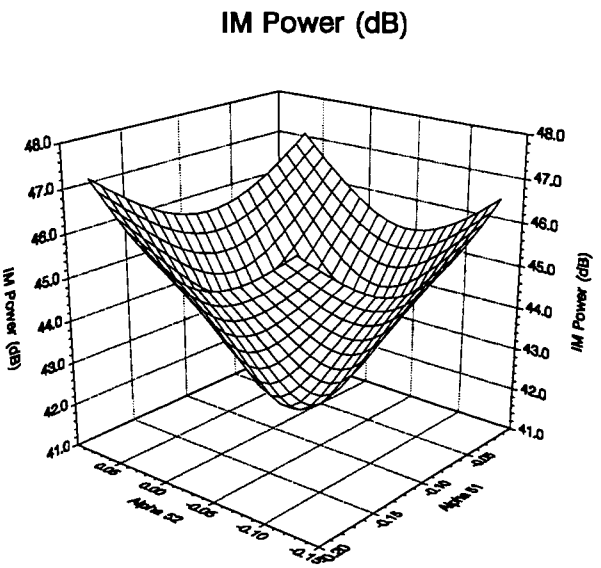

(a) Surface plot

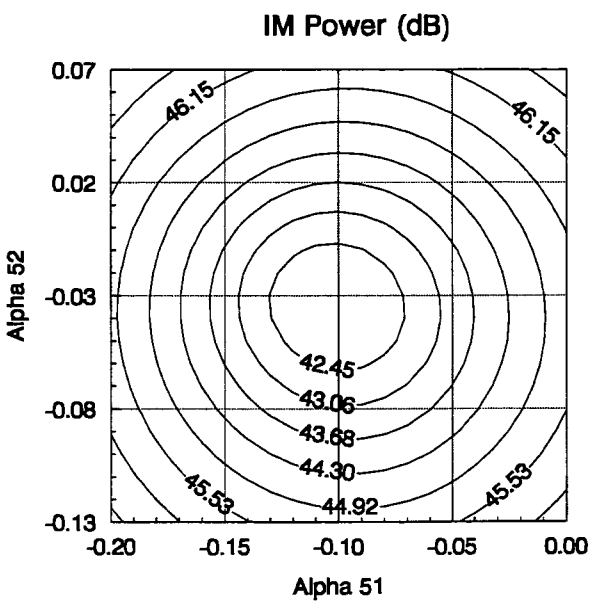

(b) Contour plot

Figure 6.2 Simulated adjacent-channel power versus α_5, OBO = 2 dB

6.2 Adaptation of Postdistorter Coefficients

The results in this section are divided into two parts. Section 6.2.1 demonstrates the postdistorter adaptation based on the IM power method (Section 4.1). Section 6.2.2 presents the adaptation results based on the variance method (Section 4.2). In principle, whichever adjacent channel has higher inband power will be the dominant contributor to the adjacent channel interference. Hereafter, it is reasonable to consider the case of a desired channel and a single adjacent channel only. The worst case is that both adjacent channels have the same power; then the total adjacent-channel power will be that of the single adjacent-channel case plus 3 dB. For each power measurement, 1000 symbols were generated randomly for each channel.

6.2.1 IM Power-Based Results

This section demonstrates the IM power-based adaptation and the effect of postdistortion technique on out-of-band power. The simulation models shown in Figures 5.1 and 5.3 were used to measure the out-of-band power produced by a single adjacent channel only, once again channels 1 and 2 were off but channel 3 on.

The results are shown in Figures 6.3 to 6.5 for three different OBO values of 2, 5 and 10 dB, respectively. The figures show that postdistortion indeed reduced the out-of-band power, in the desired channel's bandwidth, by up to 10, 22 and 15 dB for OBO's of 2, 5 and 10 dB, respectively. As expected, the reduction in out-of-band power increases with the increase in OBO level. But this reduction is also limited by the noise floor of the received signal. That is exactly the case for OBO of 10 dB shown in Figure 6.5, the attainable out-of-band reduction was only 15 dB instead of 22 dB as might be expected. Note that these simulated spectra were measured at point B of the receiver

model shown in Figure 5.3. The power in the bandwidth of the adjacent channel itself was caused by the postdistorter coefficients α_3 and α_5. This inband power can be reduced by optimizing α_1 and filtering using LPF #2.

The postdistorter worked best for OBO of 5 dB (or higher OBO). It is interesting to notice that postdistortion can reduce the adjacent channel power down to the noise floor for a system operating with a large OBO as illustrated in Figure 6.5. However, when the amplifier is driven very hard towards saturation (OBO = 2 dB or less), it is more difficult for the postdistorter to completely cancel the out-of-band power. One reason is that the postdistorter was modelled as a 5th order polynomial. Therefore, to improve the out-of-band reduction at small OBO power levels one can use a higher order (7th or 9th) polynomial for the postdistorter, unfortunately this will increase the complexity and convergence time. One can compromise by backing off the amplifier output power with the benefits of simplicity and fast convergence. From this point on, the amplifier's OBO was selected at 5 dB, unless stated otherwise. After the postdistorter converges, reception of the desired channel can then be established with optimal adjacent-channel interference.

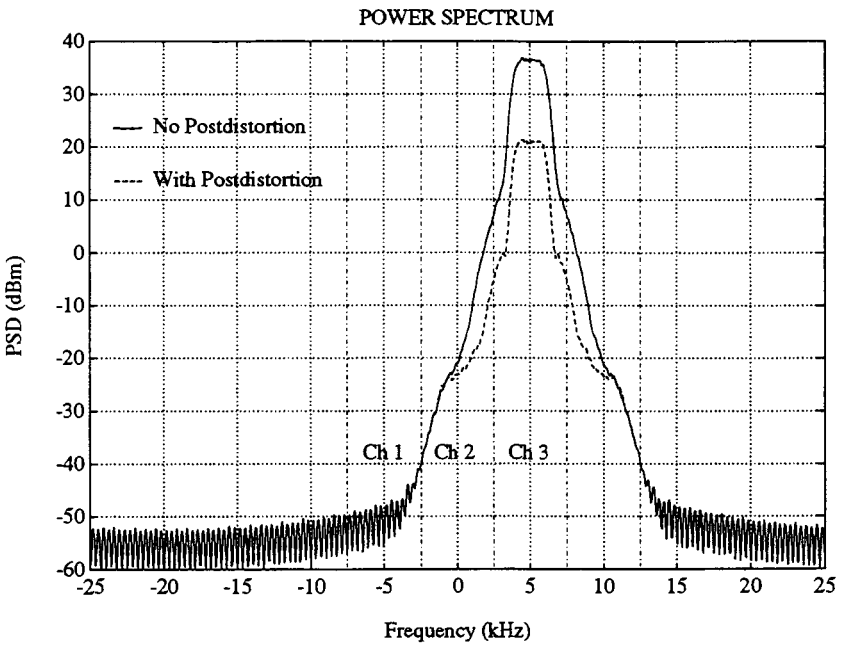

Figure 6.3 Simulated power spectrum with IM power method, OBO = 2 dB

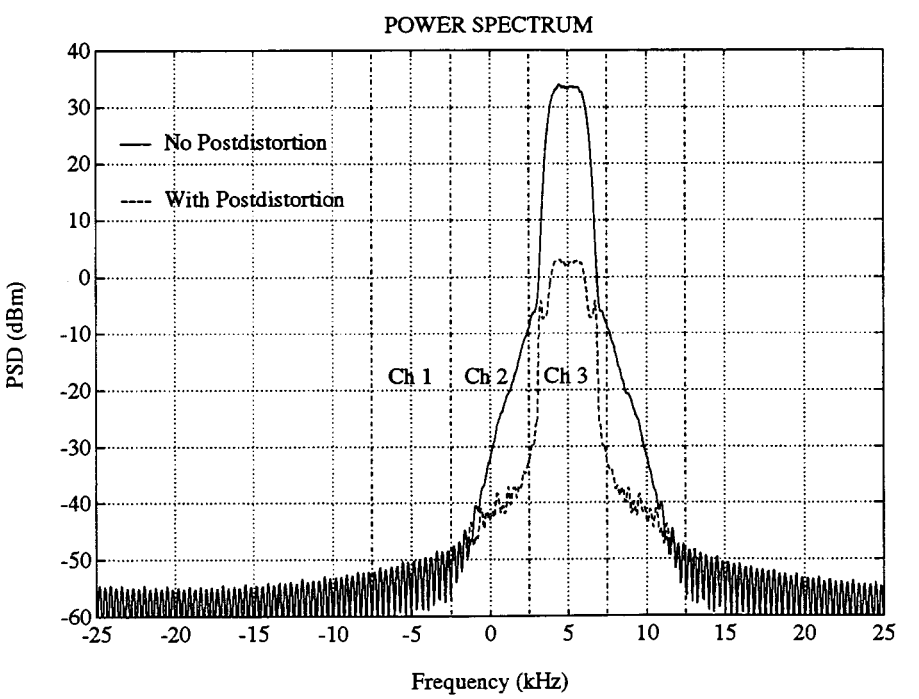

Figure 6.4 Simulated power spectrum with IM power method, OBO = 5 dB

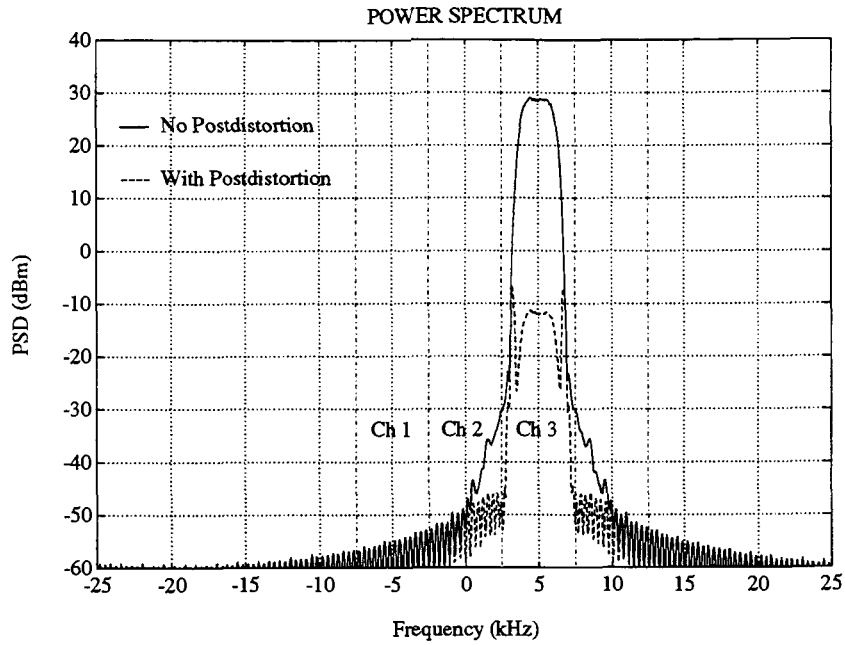

Figure 6.5 Simulated power spectrum with IM power method, OBO = 10 dB

6.2.2 Variance-Based Results

This section demonstrates the variance-based adaptation method and the effectiveness of the postdistortion technique with high adjacent-channel interference power. In this simulation, only the center channel 2 and single adjacent channel 3 were active. In order to make a manageable comparison between adaptation techniques, both amplifiers #2 and #3, were set at the same OBO of 5 dB.

The results are shown in Figures 6.6 to 6.11 for different C/Ca ratios of -40, -50 and -60 db, respectively; where C/Ca is the ratio of the desired channel's peak power to the adjacent channel's peak power. Figures 6.6, 6.8 and 6.10 show the constellations of the system with C/Ca ratios of -40, -50 and -60 dB, respectively. Figures 6.7, 6.9 and 6.11 show the power spectra of the system with C/Ca ratios of -40, -50 and -60 dB,

respectively. Recall that the variance-based method optimizes the postdistorter coefficients for minimal constellation variance, the power spectrum is evaluated to confirm reduction of adjacent channel power.

The figures show that the variance-based adaptation indeed reduced the constellation variance; consequently the out-of-band power dropped by up to 20 dB for all three cases. Interestingly enough, even though the desired channel is buried in the adjacent channel interference (Figures 6.9 and 6.11), the postdistortion technique can still adapt and reduce the adjacent channel's power.

There is a 2 dB difference in IM power reduction between the power-based and variance-based methods for the case of 5 dB OBO. The main reason is that by measuring the adjacent channel power during the off-time of transmitter #2, the power-based method has perfect information about the out-of-band power function to adapt the postdistorter coefficients. Whereas in the variance-based method, the adjacent channel's power acts as a noise source in estimating the out-of-band power function. In other words, the variance-based method does not have perfect information about the adjacent channel which is the usual case in practice. This implies that the variance-based method is the more practical system.

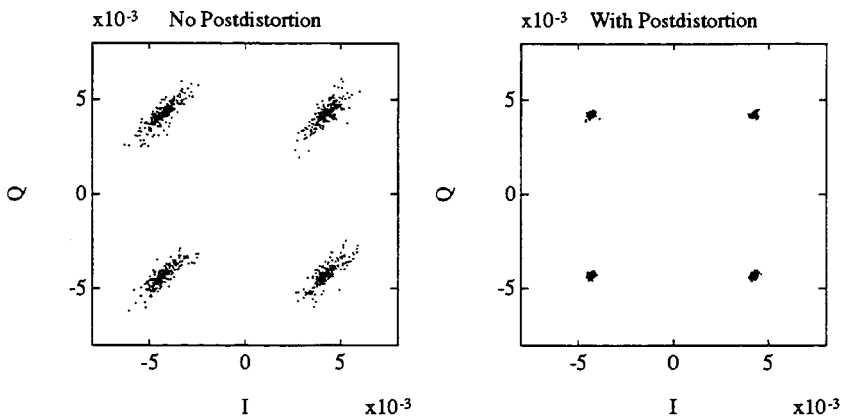

Figure 6.6 Simulated constellation, C/Ca = -40 dB

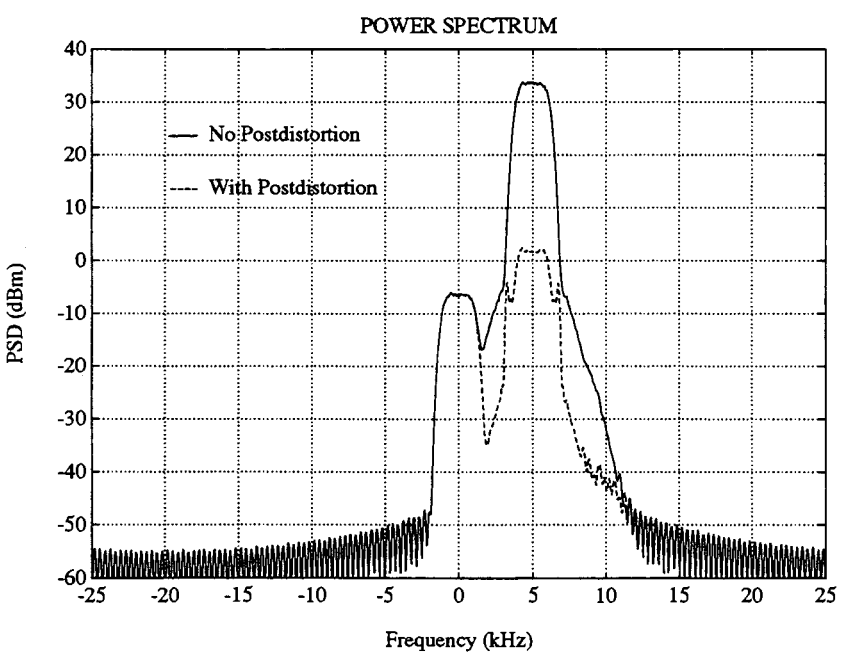

Figure 6.7 Simulated power spectrum with variance method, C/Ca = -40 dB

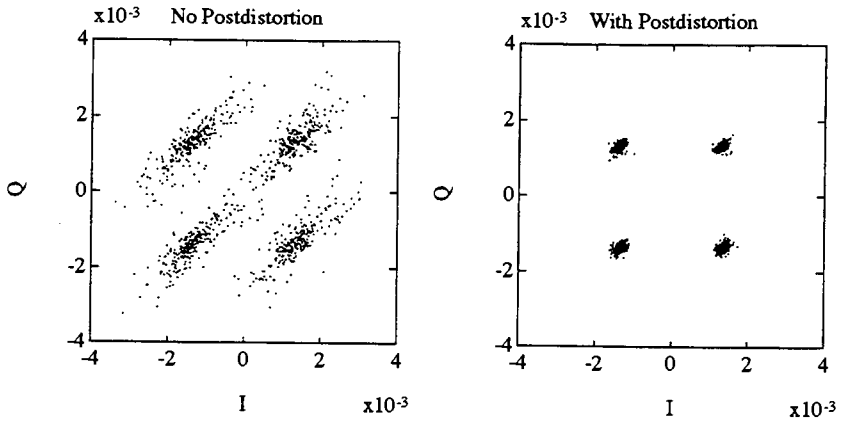

Figure 6.8 Simulated constellation, C/Ca = -50 dB

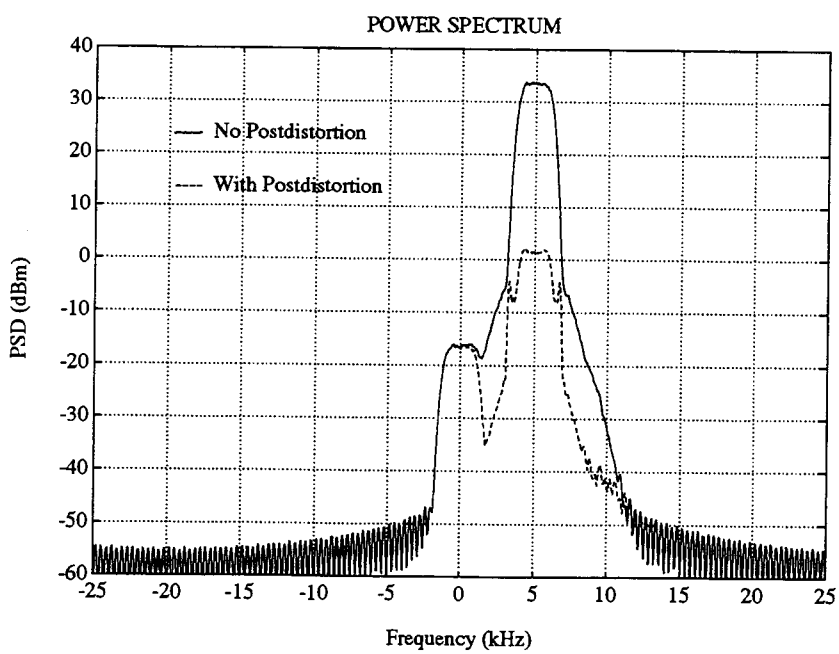

Figure 6.9 Simulated power spectrum with variance method, C/Ca = -50 dB

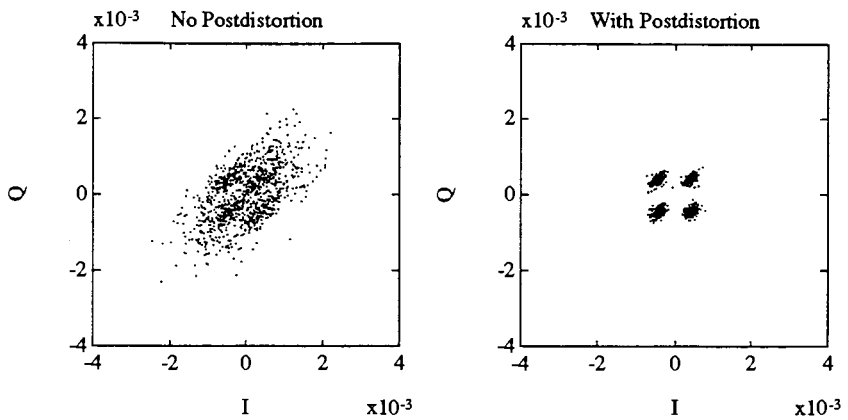

Figure 6.10 Simulated constellation, C/Ca = -60 dB

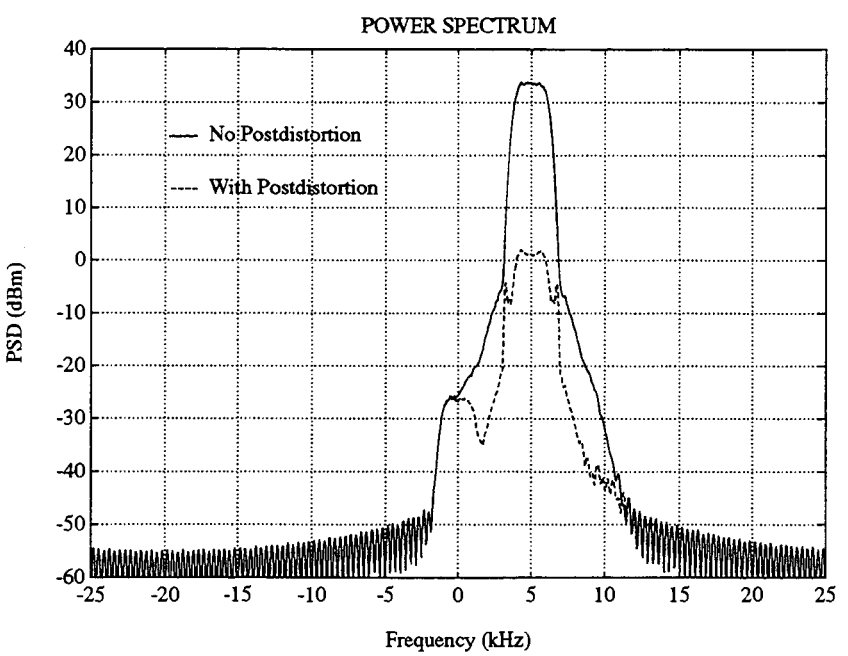

Figure 6.11 Simulated power spectrum with variance method, C/Ca = -60 dB

6.3 System Performance

The results in this section are divided into three parts. Section 6.3.1 demonstrates the effect of postdistortion on SNR. Section 6.3.2 presents the convergence speed of the postdistorters. Section 6.3.3 considers the system performance in channel fading conditions.

6.3.1 Signal-to-Noise Ratio

This section demonstrates the effect of postdistortion on SNR. Figure 6.12 shows SNR versus C/Ca ratio for various amplifier's OBO values. Recall that the power spectrum of intermodulation (IM) products caused by the amplifier nonlinearities covers the inband frequencies as well as the out-of-band frequencies. These inband IM products can be treated as a noise source which generates the equivalent inband noise power, as contrast to out-of-band (noise) power or adjacent channel power caused by an adjacent channel's amplifier. At high C/Ca ratios - for instance, higher than -30 dBc for 2-dB OBO curve - the inband noise power dominates the adjacent channel power; hence SNR of the center channel depends primarily on its own inband noise power, and is almost constant. At low C/Ca ratios, the adjacent-channel power dominates the inband noise power; consequently, SNR decreases as the peak power of the desired channel reduces. As expected, SNR increases as the amplifier's OBO increases. That is, as the amplifier operates further in the linear region, there will be less nonlinear distortion generated, and hence higher SNR.

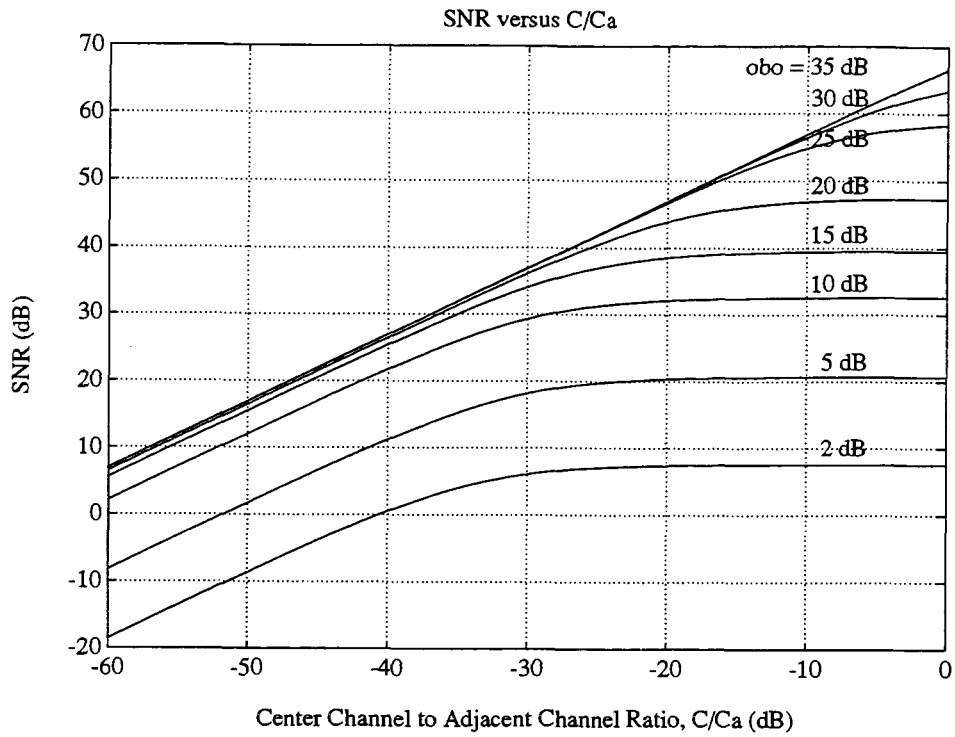

Figure 6.12 SNR due to adjacent channel power

Figure 6.13 illustrates the effect of postdistortion on SNR for three different OBO values of 2, 5 and 10 dB. The postdistortion technique improves SNR most when the peak power of the desired channel is much less than that of the adjacent channel. As explained above, the adjacent channel power is the dominant noise power at low C/Ca ratios, and recall that the postdistortion's goal is to reduce the adjacent channel power. Therefore, the postdistortion technique has the most effect on SNR at low C/Ca ratios, exactly when improvement is most needed. Or equivalently, postdistortion increases the system dynamic range, at low C/Ca ratios.

As explained in Section 6.2.1, the reduction of out-of-band power is limited by the system noise floor, so is the system SNR. From Figure 6.13, the system SNR increases as the OBO level increases until the system noise floor limits any improving in SNR for

high OBO levels (see SNR curves with 10-dB OBO). It is possible that if the noise floor is reduced, one can attain further improvement in SNR for high OBO's. It is interesting to notice that a system with 5-dB OBO improves the system SNR the most. This brings out the trade-off issues in system design. How far the system output should be backoff before its power efficiency becomes undesirable. In subsequent sections, OBO between 3 and 5 dB have been selected.

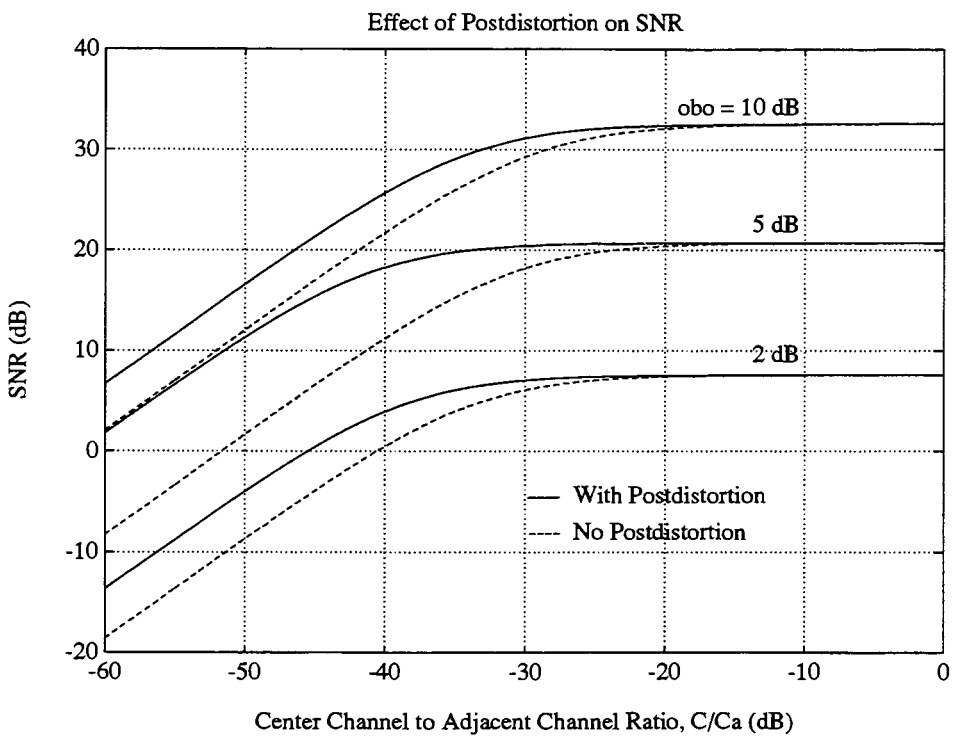

Figure 6.13 Effect of postdistortion on SNR

6.3.2 Convergence Speed

The simulated convergence speed is shown in Figures 6.14 for a system with 5 dB OBO. In this simulation, the SNR was calculated for every 1,000 symbols (per iteration). As shown in Figure 6.14, the system started without postdistortion for the first 40

iterations, then postdistortion was switched on afterwards. The system SNR converged after about 80 iterations or approximately 32 seconds for the given symbol rate of 2,500 symbols/s. Faster convergence can be achieved by using more complex adaptive algorithms which takes into account the quadratic nature of the adjacent channel power with respect to the postdistorter coefficients [10,12], or using a smaller number of samples per iteration.

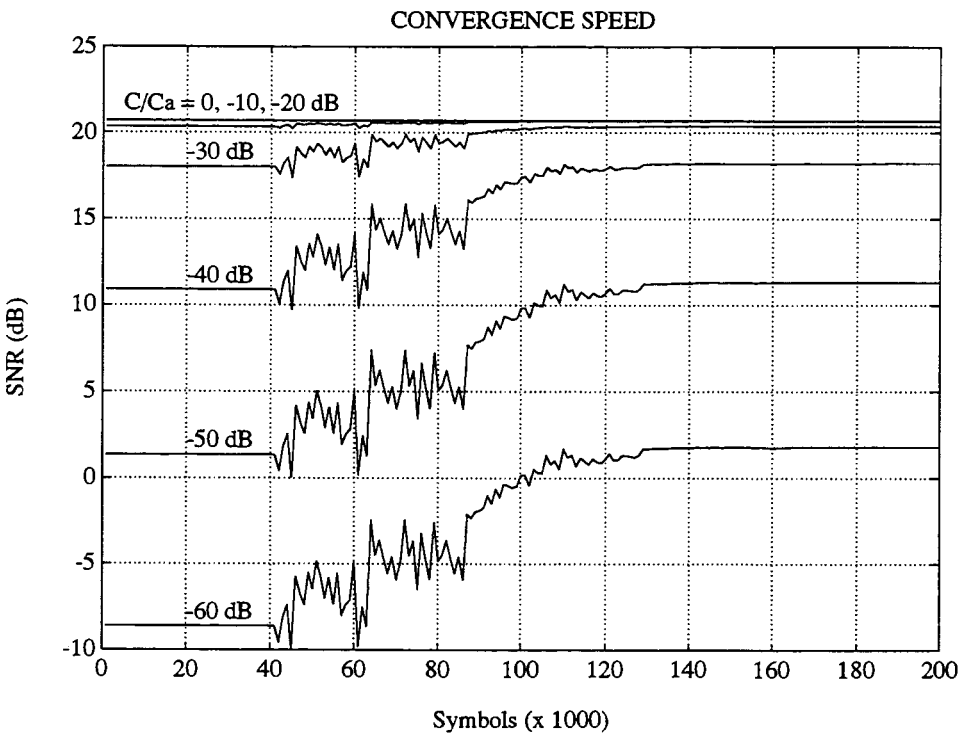

Figure 6.14 Simulated convergence speed, OBO = 5 dB

6.3.3 In Fading Channel Conditions

This section discusses the system performance in fading channel conditions which is an inevitable problem in mobile communications. Channel fading or multipath fading is a phenomenon in which a transmitted radio signal is attenuated and reflected in

different paths by obstructions, then these signals are recombined at the receiver constructively or destructively. A typical received signal power in fading conditions is shown in Figure 6.15. Points A, B and C depict received signal powers in decreasing order of fading level. The normalized duration of fades [15] is shown in Figure 6.16. For a vehicle travelling at 50 km/h, and the carrier frequency of 850 MHz, the maximum Doppler frequency f_m is about 40 Hz, and the duration of fades below -20 dB is less than 1 ms. This means that deep fades happen very briefly and infrequently. Only flat fading is considered in this thesis, the effect of frequency-selective fading on the postdistortion receiver will be the subject for future work. This section is divided in two parts. The first part considers the effects of channel fading on mobile receivers, and the second part on base-station receivers.

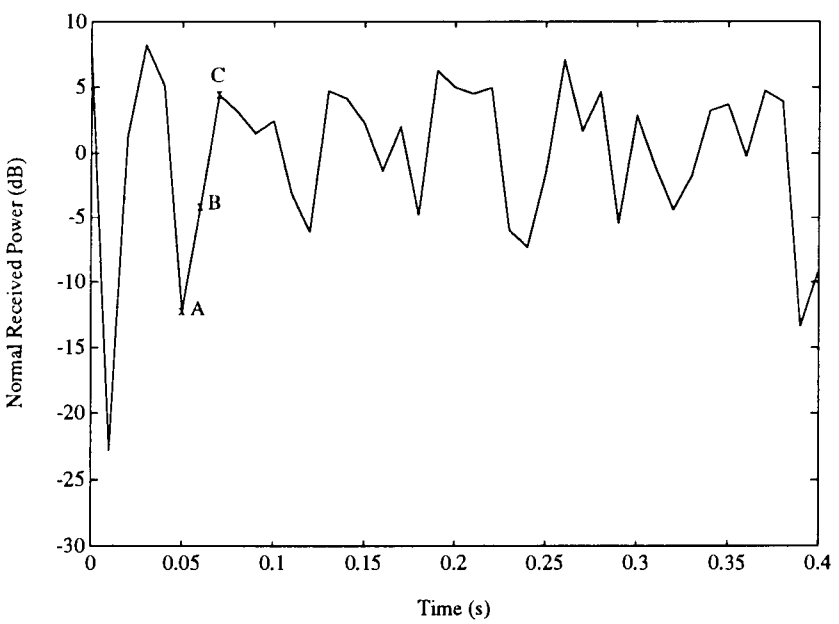

Figure 6.15 Typical received power in channel fading conditions

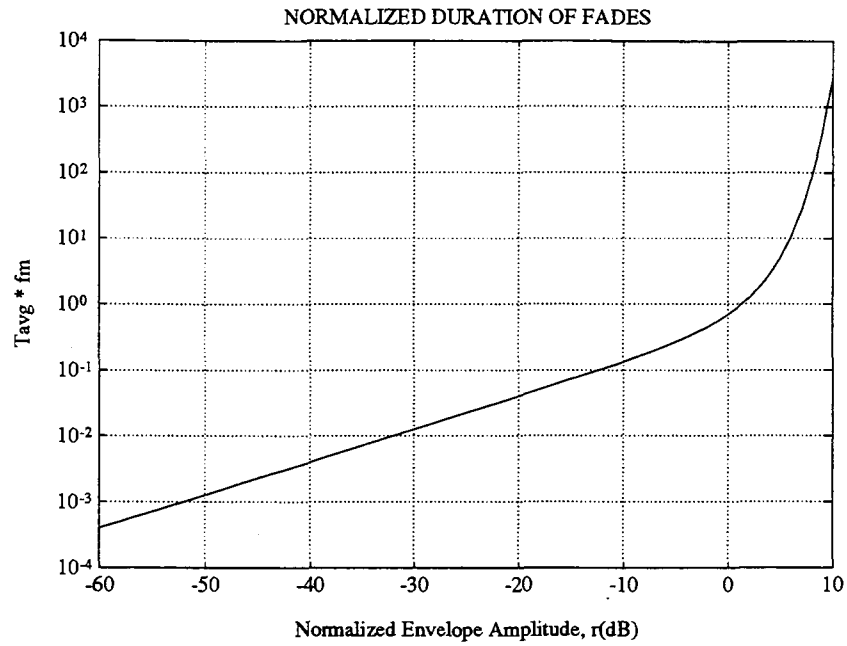

Figure 6.16 Normalized duration of fades

The effects of channel fading on mobile receivers is considered first. Recall that the base stations will still transmit 'clean' signals with -60 dBc out-of-band emission as required by FCC regulations; only the mobile units are allowed to transmit with a higher level of out-of-band emission, say -45 dBc. In other words, postdistortion is an one-way operation. Therefore, channel fading will affect the mobile receivers in the same way as if postdistortion is applied or not. In other words, compared with regular systems, postdistortion provides the same performance for mobile units in fading conditions. Extensive research on channel fading on mobile units can be found in the literature [15,16].

Second, the following subsections consider the effects of channel fading on the base-station receivers using postdistortion. Recall that the postdistortion receiver is concerned with three main signals: a center channel signal and two adjacent channel

signals. The received signals are assumed to experience fading independently. The trivial case is when all 3 channels experience the same fade, under this condition the postdistorter coefficients will not change. As previously assumed, fading is flat and extends over the three channel bandwidths. Three cases will be considered in increasing order of severeness: only adjacent channels in fades, all three channels in fades, and only the center channel in a fade. Figure 6.17 depicts all three situations.

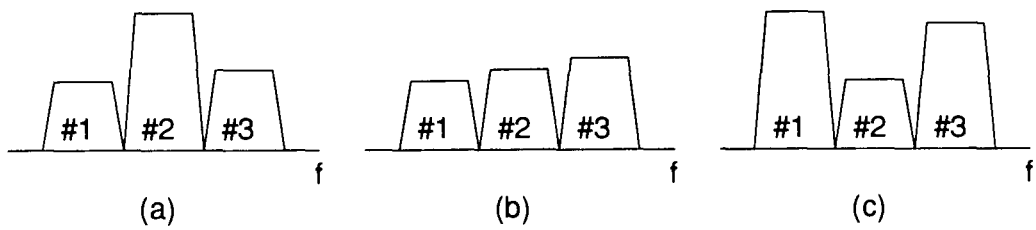

Figure 6.17 Various situations of channel fading

6.3.3.1 Adjacent Channels in Fades

This section considers that only adjacent channels are in fades (see Figure 6.17(a)), and is divided into two subcases. The first subcase supposes that the postdistorters are already adapted before the adjacent channels are in fading. The second subcase assumes that the postdistorters are not optimized yet when deep fades hit both adjacent channels. In either case, it is easy to see that fading is not a problem to the system performance because the adjacent channel powers are already much lower than the inband power of the center channel. Therefore the system SNR and BER will not be affected by channel fading, in this case.

6.3.3.2 Center Channel in Fades

This section considers the case that only the center channel is in fades (see Figure 6.17(c)), which is the worst case. Two subcases are considered once again. First, suppose that the postdistorters are already adapted before the center channel is hit by fading. When the center channel is in a deep fade, the system SNR will temporarily drop because of the reduction in its inband power. When the center channel gets out of the fade, the system SNR will climb back to its original value. Recall that the variance-based adaptation method (Section 4.2) continually monitors the adjacent channel powers as well as the system SNR. During the fading period, there are little variations in the adjacent channels; hence the postdistorter coefficients will be almost optimal and so will be the system SNR. For example, the SNR curve (solid line) of the postdistortion system with 5-dB OBO shown in Figure 6.13, shows that a deep fade of 50 dBc reduces the system SNR by 9 dB, whereas shallower fades (less than 30 dBc) have little effect on the system SNR. This is because the amplifier is dominated by its own IM products.

Second, suppose that the postdistorters are not optimized yet when the center channel hits a fade. Obviously, the system SNR in this case will be degraded compared to that in the former case when the system is in deep fades. For instance, the SNR curve (dash line) of no postdistortion system with 5 dB OBO shown in Figure 6.13, shows that the same deep fade of 50 dBc will reduce the system SNR by 19 dB instead of 9 dB, a 10 dB degradation in SNR. As in the former case, when the center channel gets out of fades, the system SNR will increase back to its original value. Also note that deep fades happen very infrequently and their durations are very short compared to the convergence time of the postdistorters, and hence they have little effect on the overall system performance.

6.3.3.3 All Channels in Fades

This section considers the situation that all three channels are in fades (see Figure 6.17(b)). This case is between the two previous cases, and hence the system performance is bounded by the two previous cases.

Since postdistortion is implemented at the base-station receivers, it is possible to combine the postdistortion technique with various diversity techniques to combat channel fading. This is a feature that is inconvenient and difficult to implement on portable transceivers.

6.4 System Efficiency

This section compares the transmitter's power efficiency and the spectral efficiency of the postdistortion system with those of the existing systems without postdistortion.

6.4.1 Transmitter's Power Efficiency

This section demonstrates the effect of the postdistortion technique on the transmitter's power efficiency. Figure 6.18 shows the output power and the 3rd order IM power versus input power of a typical power amplifier. As depicted in Figure 6.18, the slope of the output power and 3rd order IM power curves are 1:1 and 3:1, respectively; that is an increase (or decrease) of 1 dB in the input power will increase (or decrease) the output power by 1 dB and the 3rd order IM power by 3 dB. For simplicity, the out-of-band power will be equated to the 3rd order IM power. The simulation and measured results show that the postdistortion technique can reduce the out-of-band power by up to 20 dB for a power amplifier operating at 5-dB OBO. This implies that with an increase of 10-dB input power at the portable transmitter, the base-station receiver using

the postdistortion technique can compensate for a 30-dB increase in out-of-band power; thereby the effective out-of-band power will only increase by 10 dB, not by 30 dB as for a regular system. Therefore the postdistortion system can still achieve the same 60-dBc out-of-band emission attenuation as a regular system while allowing a 10-dB increase in the output power. With the postdistortion technique, the transmitter's power efficiency is, consequently, increased by 10 dB or by a factor of 10.

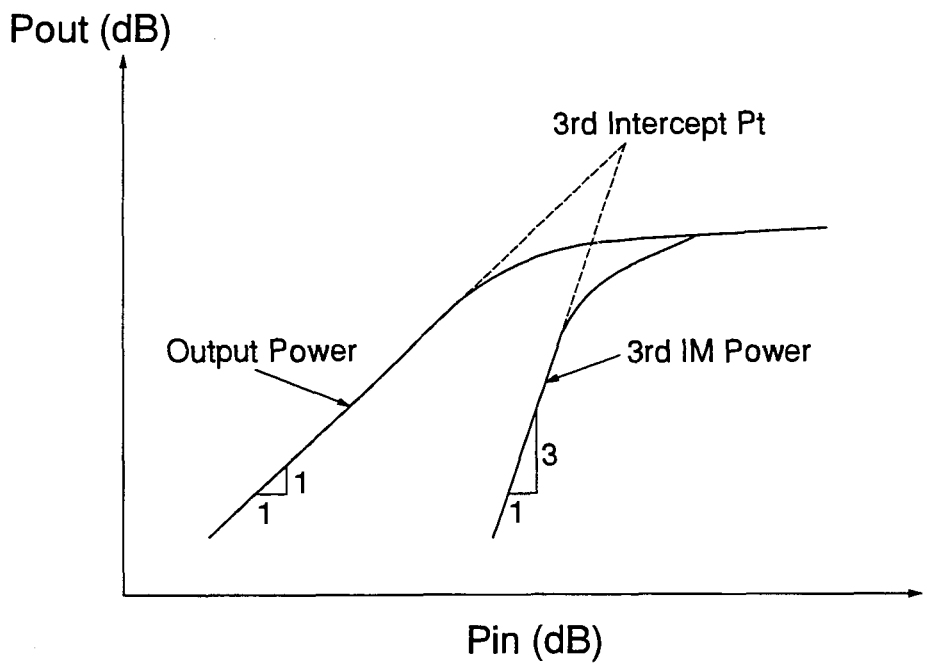

Figure 6.18 Output power and 3rd order IM power of a typical power amplifier

6.4.2 Spectral Efficiency

This section demonstrates the effect of the postdistortion technique on the spectral efficiency. The Radio Standards Specification RSS 119, Issue 3, specifies the standard channel spacing of 25 kHz for land and mobile stations operating in the 806-821 and 851-866 MHz bands. The out-of-band emission attenuation for data input is shown in

Figure 6.19.

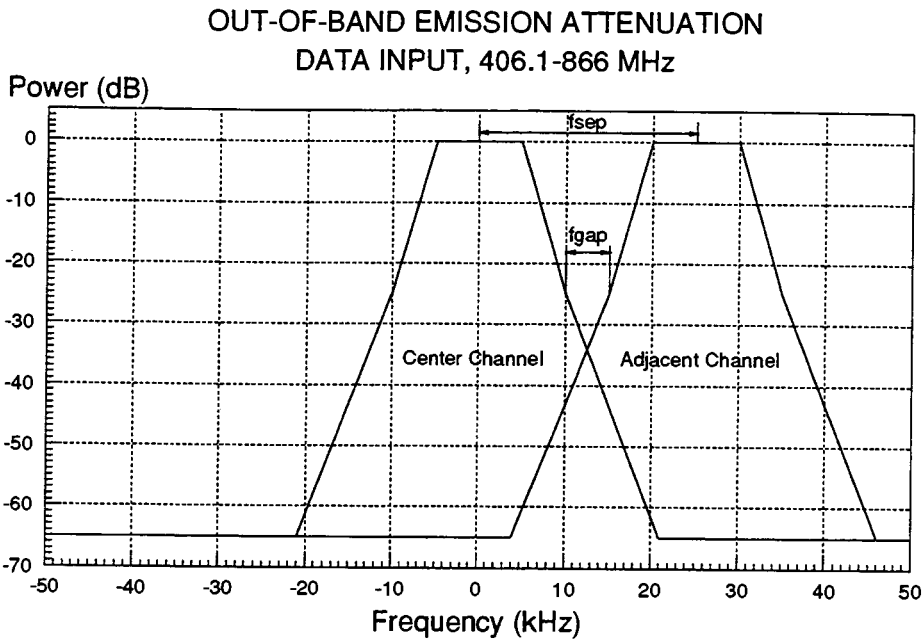

Figure 6.19 Out-of-band emission attenuation, data input, 406.1-866 MHz

As depicted in Figure 6.19, the channel spacing f_{sep} and the channel gap f_{gap} are 25 kHz and 5 kHz, respectively. The utilized spectral bandwidth f_{util} is defined as

$$f_{util} = f_{sep} - f_{gap} = 20kHz$$

The spectral efficiency of existing systems under RSS 119 standards is

$$\eta = \frac{f_{util}}{f_{sep}} = 80\%$$

Using the same channel spacing f_{sep} of 25 kHz for the postdistortion system, the resulting out-of-band emission attenuation for data input is shown in Figure 6.20.

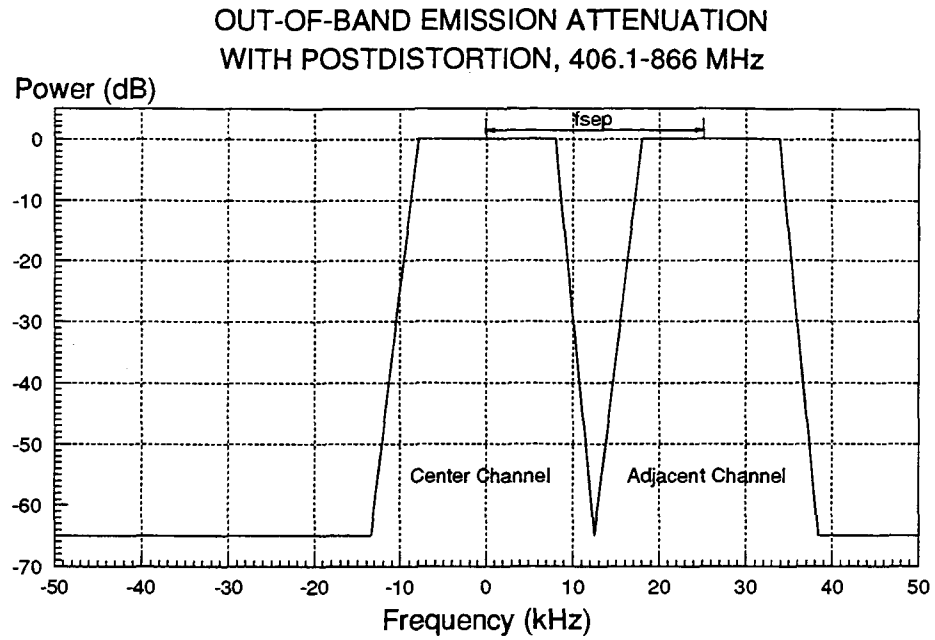

Figure 6.20 Out-of-band emission attenuation of a postdistortion system

Since the postdistortion technique can reduce the gap between adjacent channels down to 0 Hz, the utilized spectral bandwidth is maximized to the full channel bandwidth of 25 kHz. Therefore the spectral efficiency is 100% for the postdistortion system, a 20% increase in spectral efficiency over the existing system. Alternately, if the channel bandwidth is limited to 20 kHz, the number of communications channels can increase from 666 channels to 799 channels.

7 IMPLEMENTATION AND MEASURED RESULTS

This chapter describes the hardware system used to verify the analytical and simulation results. An overview of the postdistortion system design is given, followed by detailed design information and measured results. All the schematic diagrams are given in Appendix A.

7.1 System Overview

The hardware block diagram is shown in Figure 7.1. The postdistortion system consists of two major blocks, transmitter and receiver, which are described in detail in Section 7.2 and 7.3, respectively. For simplicity, only two channels, a desired channel and an adjacent channel each with a bandwidth of 5 kHz, were considered in the experiments. The adaptive control loop was not fully implemented, the postdistorter coefficients were manually adjusted for minimum IM power.

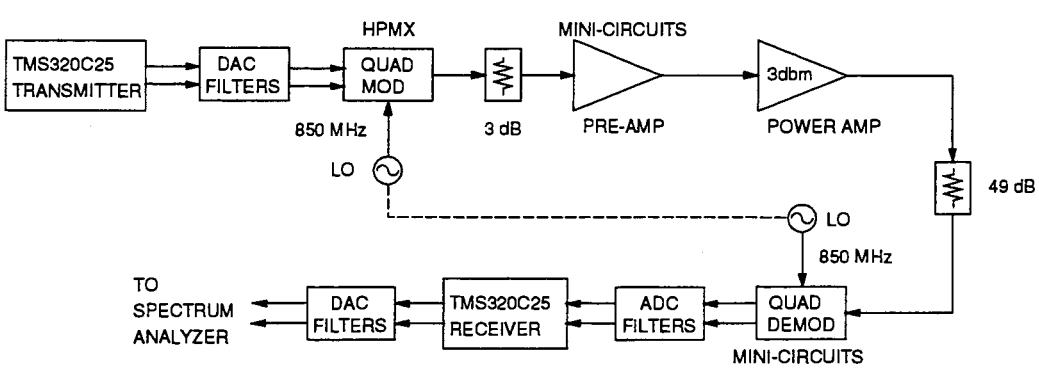

Figure 7.1 Hardware overview

7.2 Transmitter Circuit

Figure 7.2 shows the block diagram of the transmitter. A TMS320C25 system board from Spectrum Signal Processing Inc. [17] provides the transmit modem and quadrature modulator compensator [12]. The digital output from the 'C25 is converted, via two digital-to-analog converters (DACs) and two lowpass filters, to a continuous-time, analog signal. A Hewlett-Packard HPXM-2001 quadrature modulator then up-converts the baseband signal to 850 MHz. The modulated signal is fed to a Mini-Circuits [18] pre-amplifier which then drives the power amplifier - a class AB amp from 3dbm [14]. The amplifier output would normally be fed to an antenna, but for testing purposes it is attenuated before feeding directly to the receiver.

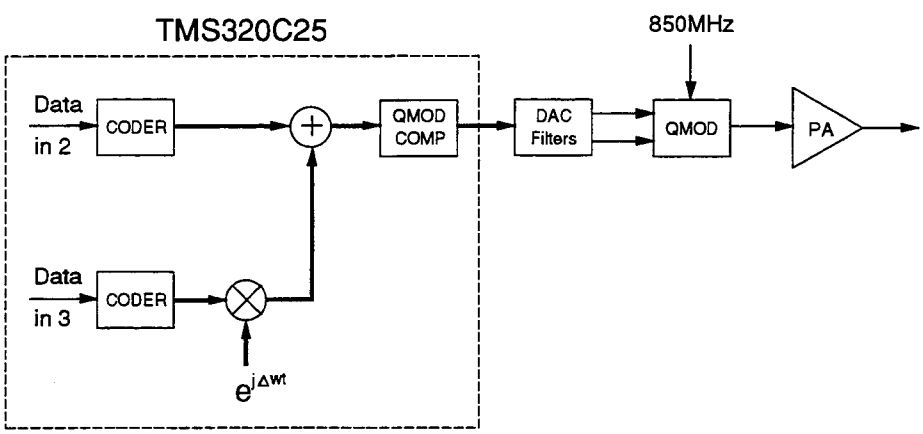

Figure 7.2 Transmitter block diagram

7.2.1 DSP Transmitter

The DSP circuit generates an offset QPSK signal for each channel according to (5.1). As presented in Section 5.1.1, the pulse is limited to 7 symbols in duration and is sampled at 20 samples per symbol. The symbol rate was 2,500 symbols per second giving a sampling rate of 50 kHz. Equation (5.1) is rather slow to implement directly in

DSP, so a look-up table method was used [12]. The look-up table method pre-calculates and stores all the 2^7 possible sequences for each output and therefore requires only a simple indexing into the table. For 20 samples/symbol and a pulse length of 7 symbols, there are $20x2^7$ words of storage. With the look-up table method, the offset QPSK signal is generated using only about 20 instruction cycles for each symbol, or about 2 μs per sample.

As depicted in Figure 7.2, the adjacent channel is shifted up in frequency by one channel bandwidth of 5 kHz, and then combined with the center channel. The combined signal is fed to a quadrature modulator compensator (QMC) to compensate for QUAD MOD errors. These errors, including DC offset, gain imbalance and phase imbalance, are caused by the QUAD MOD imperfection. Hilborn [12] successfully demonstrated the QMC model shown in Figure 7.3. The compensator calculations take only 11 instruction cycles or about 1.1 μs per sample.

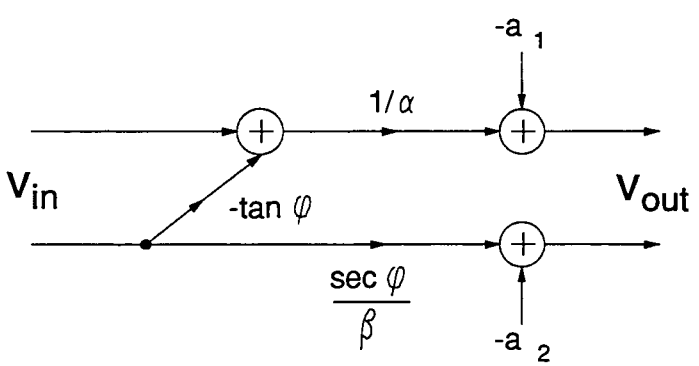

Figure 7.3 Model of a quadrature modulator compensator

7.2.2 Reconstruction Filter #1

The digital outputs from the TMS320C25 transmitter are converted to analog using two Burr-Brown [19] PCM53 DACs. Lowpass filters were used to reconstruct the analog

signal. The filters were 10th order Butterworth filters with 18 kHz cutoff frequency. The simulated response of the filters is shown in Figure 7.4. The measured response of the filters was very close to simulations, and the filters have less than 0.1 dB ripple in the passband.

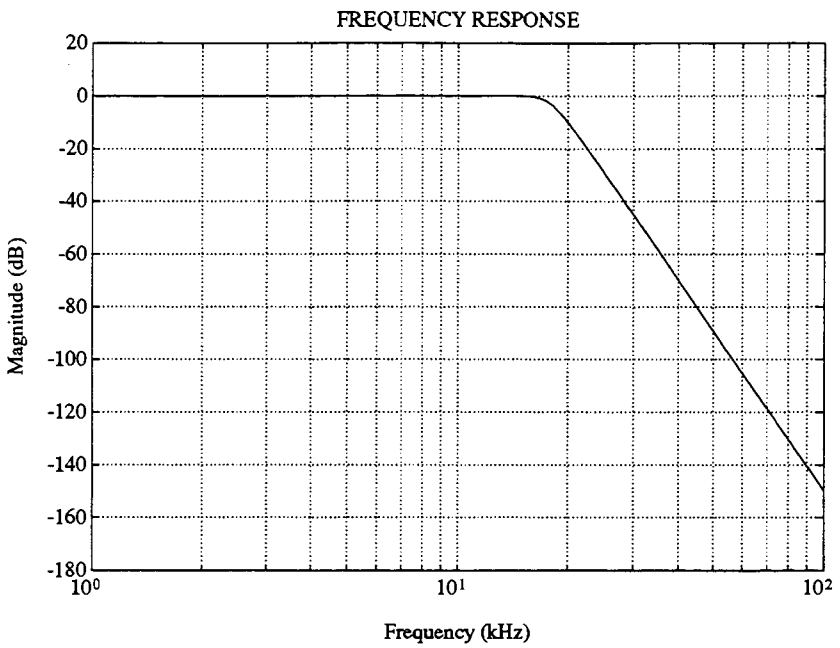

Figure 7.4 Frequency response of DAC filters #1

7.2.3 Quadrature Modulator

The quadrature modulator was constructed from a Hewlett-Packard chip, HPXM-2001, by Sirooj Rambaran (SFU, 1992). The HPMX-2001 is a silicon based bipolar monolithic quadrature phase shift keyed modulator. The chip is suitable for narrowband applications and has a typical local oscillator (LO) operating frequency range of DC-2000 MHz. The DC offset, gain, and phase characteristics of this HP modulator were reported by Hilborn [12]. The HP modulator schematic is shown in Appendix A.

7.3 Receiver Circuit

Figure 7.5 shows the block diagram of the receiver. The received signal is down-converted from 850 MHz to baseband by a quadrature demodulator (QUAD DEMOD). Similar to QUAD MOD imperfection, QUAD DEMOD imperfections also introduce DC offset, gain and phase imbalances in the demodulated signal. These QUAD DEMOD errors are then corrected by an analog QUAD DEMOD compensator (QDMC). Note that the QUAD DEMOD outputs two analog signals, the in-phase I and quadrature Q components. The corrected signals are lowpass filtered to prevent frequency aliasing before they are converted to digital signals by two analog-to-digital converters (ADCs). A TMS320C25 system board performs postdistortion on the digitized signals. The postdistorted signals are then converted to analog signals via two DACs and two lowpass filters. The output signals would normally be fed to a decision block to recover the transmitted bits, but for testing purposes they are coupled to a spectrum analyzer.

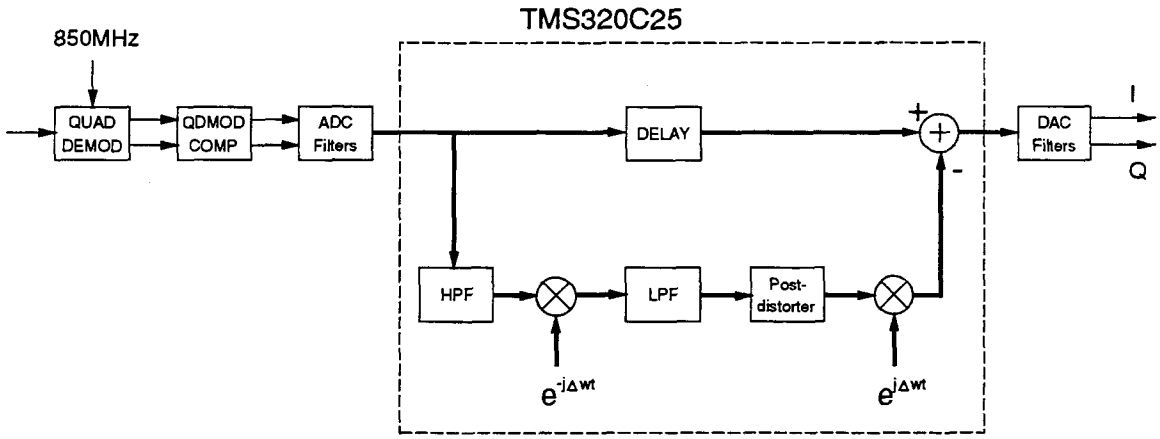

Figure 7.5 Receiver block diagram

7.3.1 Quadrature Demodulator

The quadrature modulator was built from Mini-Circuits parts by Sirooj Rambaran (SFU, 1992). These components include:

mixers	SRA-2CM
0° power splitter	PSC-2-4
lowpass filters	PLP-10-7

An additional 90° power splitter was custom designed by S. Rambaran.

7.3.2 Analog Quad Demod Compensator

The demodulated signals are corrected for QUAD DEMOD errors by the QDMC shown in Figure 7.6. The circuit schematic is shown in Appendix A. The derivation for QUAD DEMOD correction is given in Appendix B.

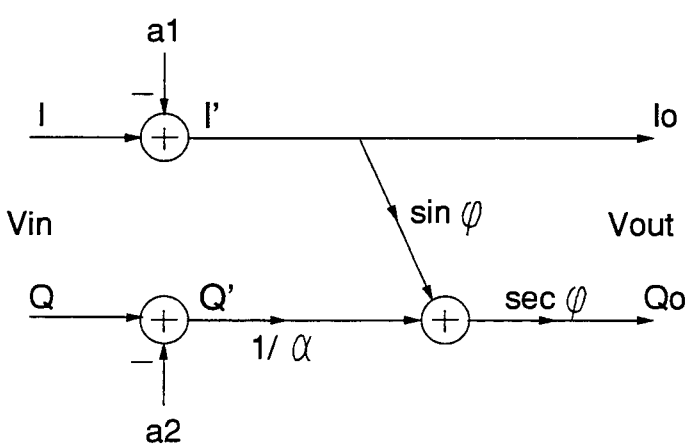

Figure 7.6 Model of an analog QUAD DEMOD compensator

7.3.3 Anti-aliasing Filter

The compensated signals are lowpass filtered to prevent frequency aliasing which would occur with discrete-time signals. The anti-aliasing filters were 4th order

Butterworth filters with 20 kHz cutoff frequency. The simulated response of the filters is shown in Figure 7.7. The measured response of the filters was very close to simulations, and the filters have less than 0.1 dB ripple in the passband.

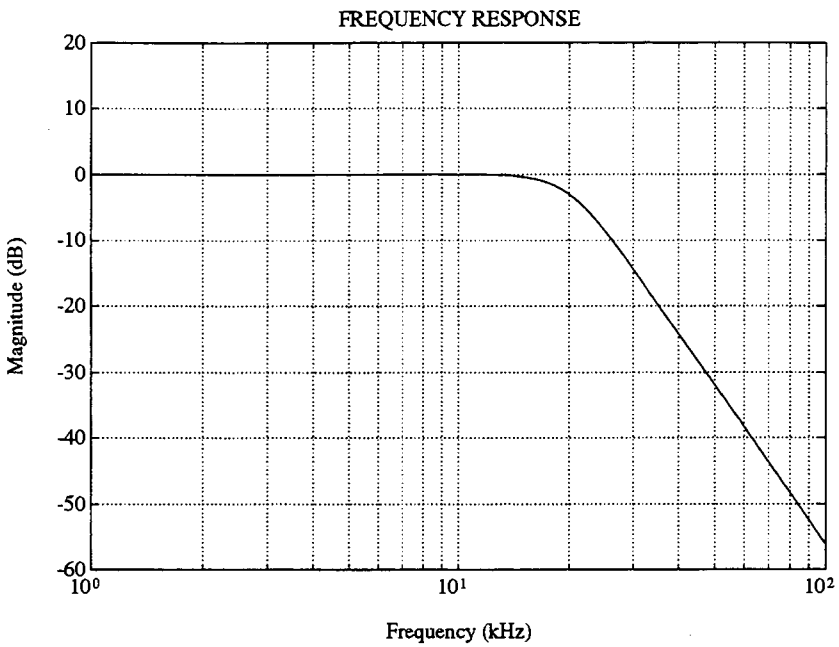

Figure 7.7 Frequency response of ADC filters

7.3.4 DSP Receiver

The filtered signals are sampled at 25 kHz by two sample-and-hold SHC5320's [19] and alternately quantized by a single Burr-Brown PCM75 ADC. The digitized signals are then divided into two branches as depicted in Figure 7.8. Note that the block diagram of the DSP receiver is similar to the simulation model, shown in Figure 5.3, with the exception that LPF #3 in the simulation model is replaced by HPF and LPF blocks. Splitting LPF #3 to two filters results in shorter filter lengths. In fact, the HP and LP filters are finite-impulse response (FIR) filters with respective lengths of 83 and 21. The simulated response of these filters are shown in Figure 7.9.

In the top branch the input samples are delayed by the total delays of the combined HPF and LPF. Since the delays of HPF and LPF are 41 and 10 samples, respectively, the total delay is 51 samples. In the bottom branch the input samples are highpass filtered, shifted down in frequency by 5 kHz, lowpass filtered, distorted, and then shifted up in frequency by 5 kHz. Note that the LPF delay will cause a phase shift in the up-converted samples. To compensate for this phase shift, the LO of the up converter must be delayed by the same delay of LPF (see derivation in Appendix C). The LPF length was selected such that with the required delay, the phase shift of the up-converter is a multiple of 2π. Therefore the phase delay of the up converter is transparent. Consequently, no LO delay was done explicitly. The up-converted samples are then subtracted from the delayed samples, and they are output at the sampling rate of 25 kHz. The complete operation takes about 189 instruction cycles or about 18.9 μs.

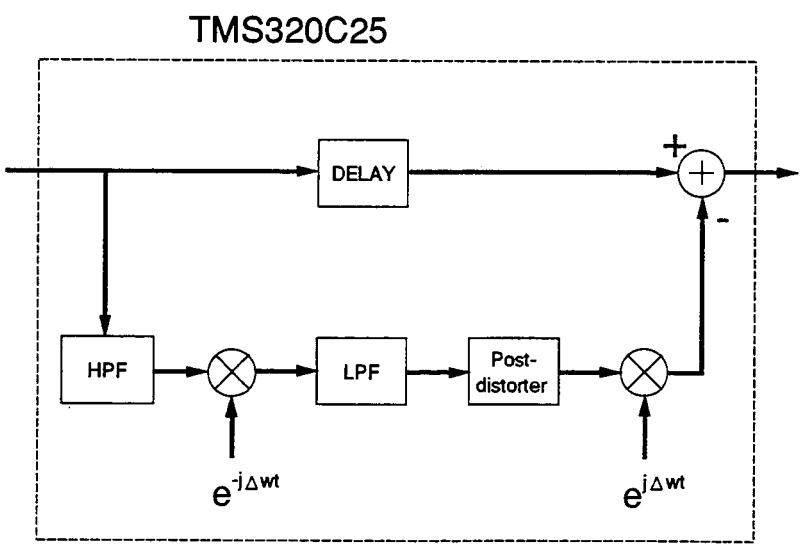

Figure 7.8 DSP receiver block diagram

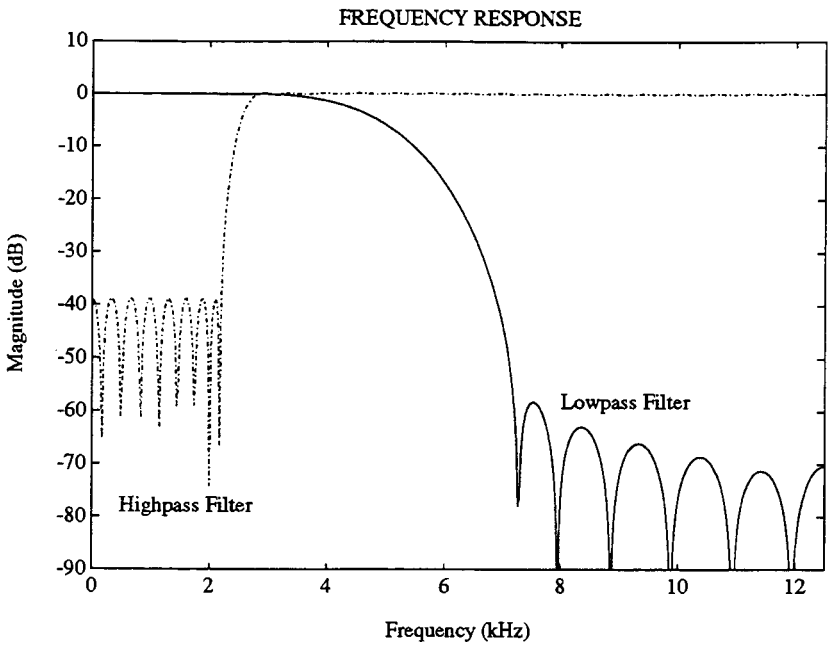

Figure 7.9 Simulated response of HP and LP filters

7.3.5 Reconstruction Filter #2

The digital outputs from the TMS320C25 receiver are converted to analog signals using two Burr-Brown PCM53 DACs. Lowpass filters were used to reconstruct the analog signals. The filters were 8th order Butterworth filters designed with 8.5 kHz cutoff frequency. The simulated response of the filters is shown in Figure 7.10. The measured response of the filters was very close to simulations, and the filters have less than 0.1 dB ripple in the passband.

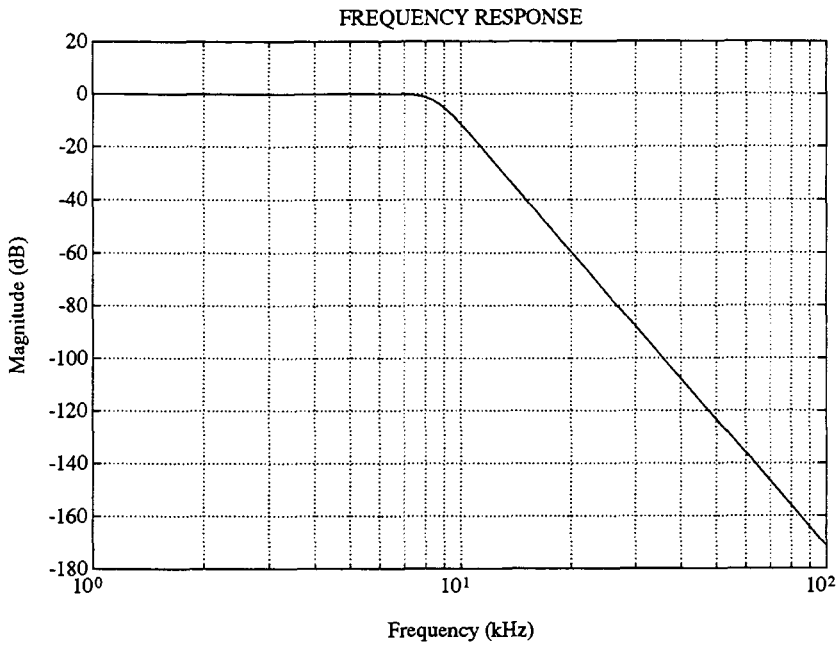

Figure 7.10 Frequency response of DAC filters #2

7.4 Measured Results

The measured power spectra with the power-based method are shown in Figures 7.11 and 7.12 for OBO of approximately 3.3 and 5 dB, respectively. In these experiments, the postdistorter coefficients were manually adjusted for minimum IM power. Note that the desired channel frequency is allocated from -2.5 to 2.5 kHz, and the adjacent channel frequency is allocated from 2.5 to 7.5 kHz. As shown in the figures, the postdistortion technique indeed reduced the adjacent channel power by approximately 15 and 10 dB, respectively, at 2.5 kHz - the channel edge. Within the bandwidth of the desired channel, the adjacent channel power has been reduced almost to the noise floor in both cases, which gives a dynamic range of about 60 dB for the desired channel. The postdistorter coefficients for the measured results are given in Table 7.1.

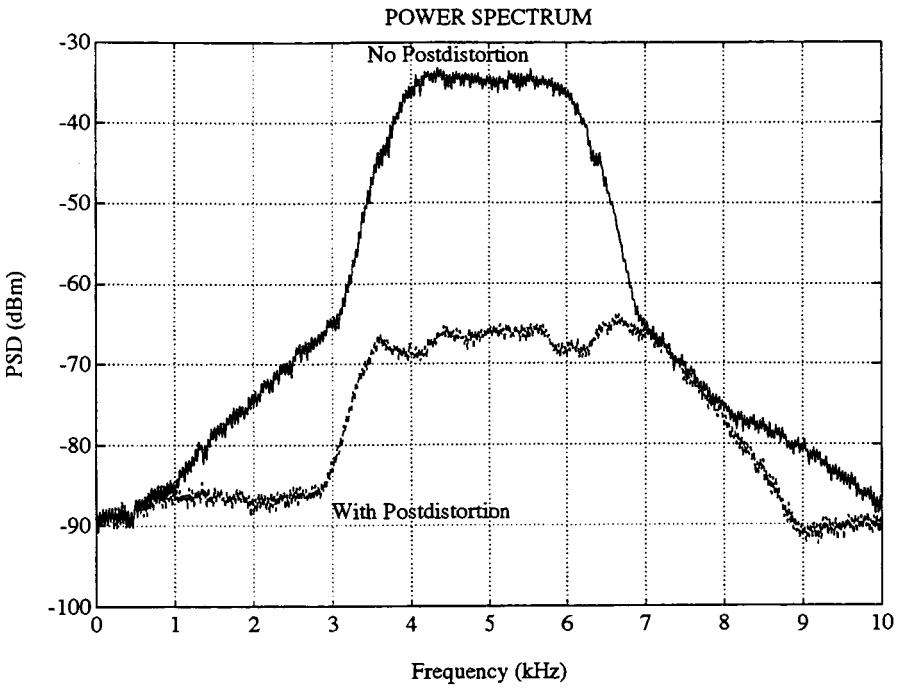

Figure 7.11 Measured power spectrum, OBO = 3.3 dB

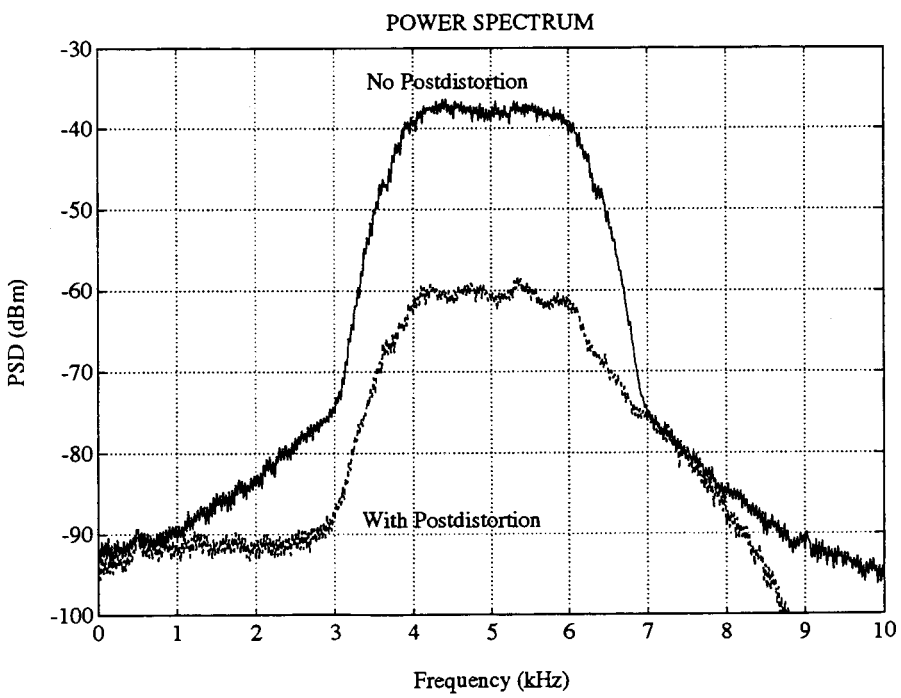

Figure 7.12 Measured power spectrum, OBO = 5.0 dB

Table 7.1 Postdistorter Coefficients for Measured Results

Postdistorter	**Output Back-Off**	
Coefficients	**OBO = 3.3 dB**	**OBO = 5.0 dB**
α_{11}	1.111	1.111
α_{12}	0.059	0.059
α_{31}	-0.148	-0.117
α_{32}	-0.0746	-0.0446
α_{51}	-0.0009	-0.0009
α_{52}	-0.0009	-0.0009

8 CONCLUSIONS

A unique postdistortion system is demonstrated to improve both the spectral efficiency and power efficiency in mobile communications. Postdistortion technique provides the potential for smaller, cheaper, and more power-efficient transmitters through compensation for AM-AM and AM-PM nonlinearities of transmitter's amplifier, at the base-station receiver.

This thesis has three main contributions. First, analysis is presented which shows that the adjacent channel power is a quadratic function of both the amplifier and postdistorter coefficients. Both simulation and measured results confirm the quadratic nature of adjacent-channel interference power. Second, a new adaptation method is described, which employs the variance information of received samples to compensate for slow variations in power amplifier's characteristics. The new method can continually adapt the postdistorter coefficients without an interruption for a training period. Third, various aspects of the system performance, including SNR and convergence speed, have been simulated. The system performance in flat fading channel conditions, an inevitable problem in mobile communications, was also considered. Both the simulation and measured results show that the postdistortion technique can improve the out-of-band emission by up to 20 dB with 5-dB OBO; the corresponding increase in mobile transmitter power efficiency is approximately a factor of 10. The spectral efficiency is increased by 20% with the postdistortion implementation.

Postdistortion must be implemented on a base station, hence the complexity and cost of the base station will increase. However, these factors can be offset by simpler and

more power efficient portable transceivers. Moreover, diversity techniques can be utilized with the postdistortion technique to combat channel fading; a feature that is inconvenient to implement on portable units.

Under current FCC requirements, postdistortion will work within an allocated band provided that the channels at both ends of the allocated band are complied with FCC regulations. Possibly in the future, the implementation of the postdistortion technique will require revision of FCC regulations on out-of-band emission.

Even though some considerations on flat channel fading were given, further investigation on frequency-selective fading must be conducted to completely evaluate the performance of the postdistortion system in fading channel conditions.

REFERENCES

[1] D.R. Green Jr., "Characterization and compensation of nonlinearities in microwave transmitters," *IEEE Trans. on Comm.*, ch. 1819-2, pp.213-217, 1982.

[2] Y. Nagata, "Linear amplification technique for digital mobile communications," *Proc. IEEE Vehic. Tech. Conf.*, pp. 159-164, San Francisco 1989.

[3] F.J. Casadevall, "The LINC transmitter," *RF Design*, 99, pp. 41-48, Feb. 1990.

[4] J. Namiki, "An automatically controlled predistorter for multilevel quadrature amplitude modulation," *IEEE Trans. on Comm.*, vol. COM-31, no. 5, pp. 707-712, May 1983.

[5] T. Nojima and T. Konno, "Cuber predistortion linearizer for relay equipment in the 800 MHz band land mobile telephone system," *IEEE Trans. on Vehic. Tech.*, vol. VT-34, no. 4, pp. 169-177, Nov. 1985.

[6] J.K. Cavers, "A linearizing predistorter with fast adaptation," *40th Vehic. Tech. Conf.*, IEEE Cat. 90CH2864-4, pp. 41-47.

[7] S.P. Stapleton and F. Costescu, "Amplifier linearization using adaptive analog predistortion," *IEEE Trans. on Vehic. Tech.*, Feb. 1992.

[8] L.D. Quach, *A Linearization Technique Using Postdistortion*, B.A.Sc. Thesis, School of Engineering Science, Simon Fraser University, 1991.

[9] S.P. Stapleton and L.D. Quach, "Reduction of adjacent channel interference using postdistortion," *42nd Vehic. Tech. Conf.*, IEEE Cat. 92CH3159-1, pp. 915-918.

[10] J.G. Proakis, *Digital Communications*, 2nd ed., McGraw-Hill, New York,1989.

[11] B.D. Bunday, *Basic Optimisation Methods*, Edward Arnold Publishers Ltd., London, 1984.

[12] D. Hilborn, *An Adaptive Direct Conversion Transmitter*, M.A.Sc. Thesis, School of Engineering Science, Simon Fraser University, 1992.

[13] A.V. Oppenheim and R.W. Schafer, *Discrete-Time Signal Processing*, Prentice Hall, Englewood Cliffs, New Jersey, 1989.

[14] 3dbm Inc., Westlake Village, CA.

[15] W.C. Jakes, *Microwave Mobile Communications*, Wiley-Interscience, New York, 1974.

[16] W.C.Y. Lee, *Mobile Communications Engineering*, McGraw-Hill, New York, 1982.

[17] SPECTRUM signal Processing Inc., #301-3700 Gilmore Way, Burnaby, B.C., V5G 4M1.

[18] Mini-Circuits, Brooklyn, New York.

[19] Burr-Brown Corporation, 6730 S. Tucson Blvd., Tucson, AZ 85706.

[20] J.K. Cavers, J. Varaldi and P. Ho, "Cochannel interference and system efficiency with pilot symbol assisted Trellis coding." *1992 IEEE International Conf. Selected Topics in Wireless Comm.*, IEEE Cat. 92TH0462-2, pp. 344-347.

APPENDIX A

SCHEMATIC DIAGRAMS

This appendix shows the schematic diagrams for the implemented system. These include HP quadrature modulator, analog quad demod compensator, reconstruction filters and anti-aliasing filter.

A.1 HP Quadrature Modulator

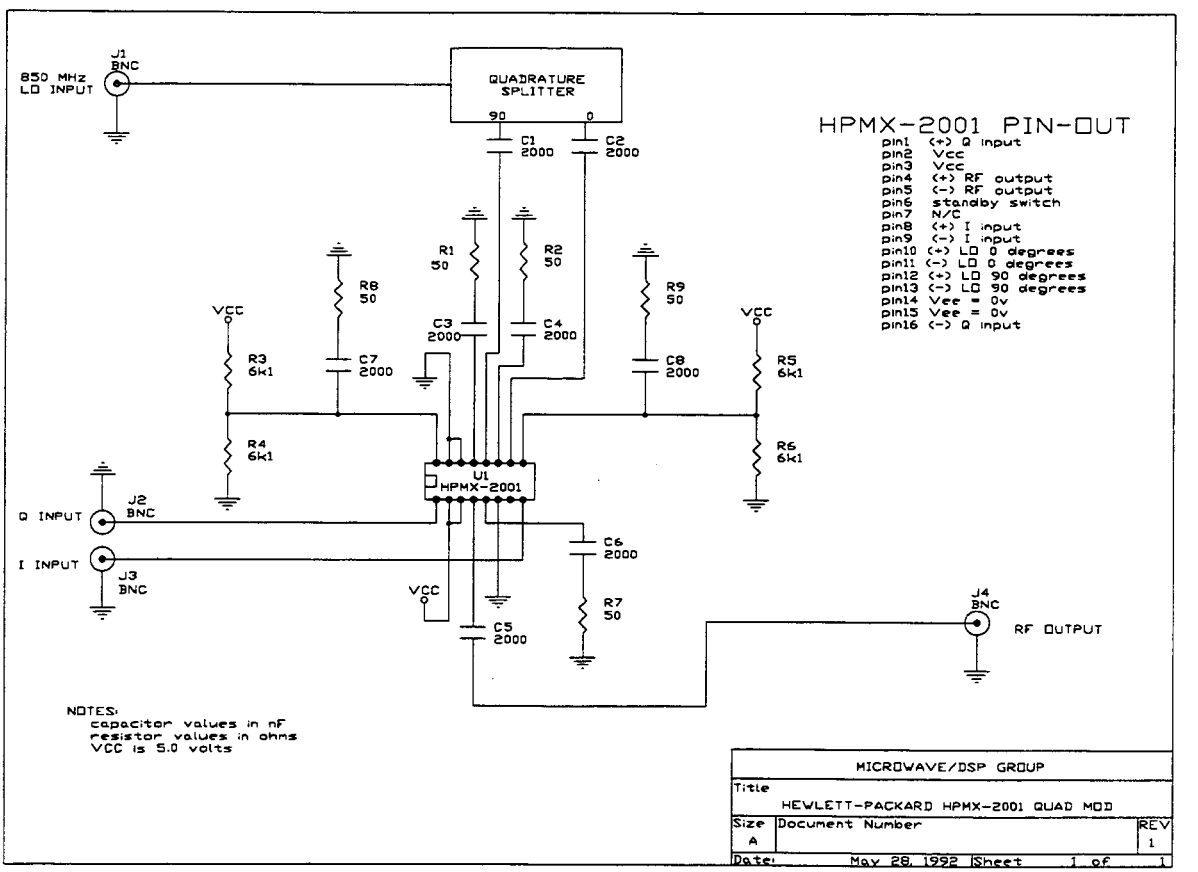

Figure A.1 HP quadrature modulator circuit

A.2 Quadrature Demodulator Compensator

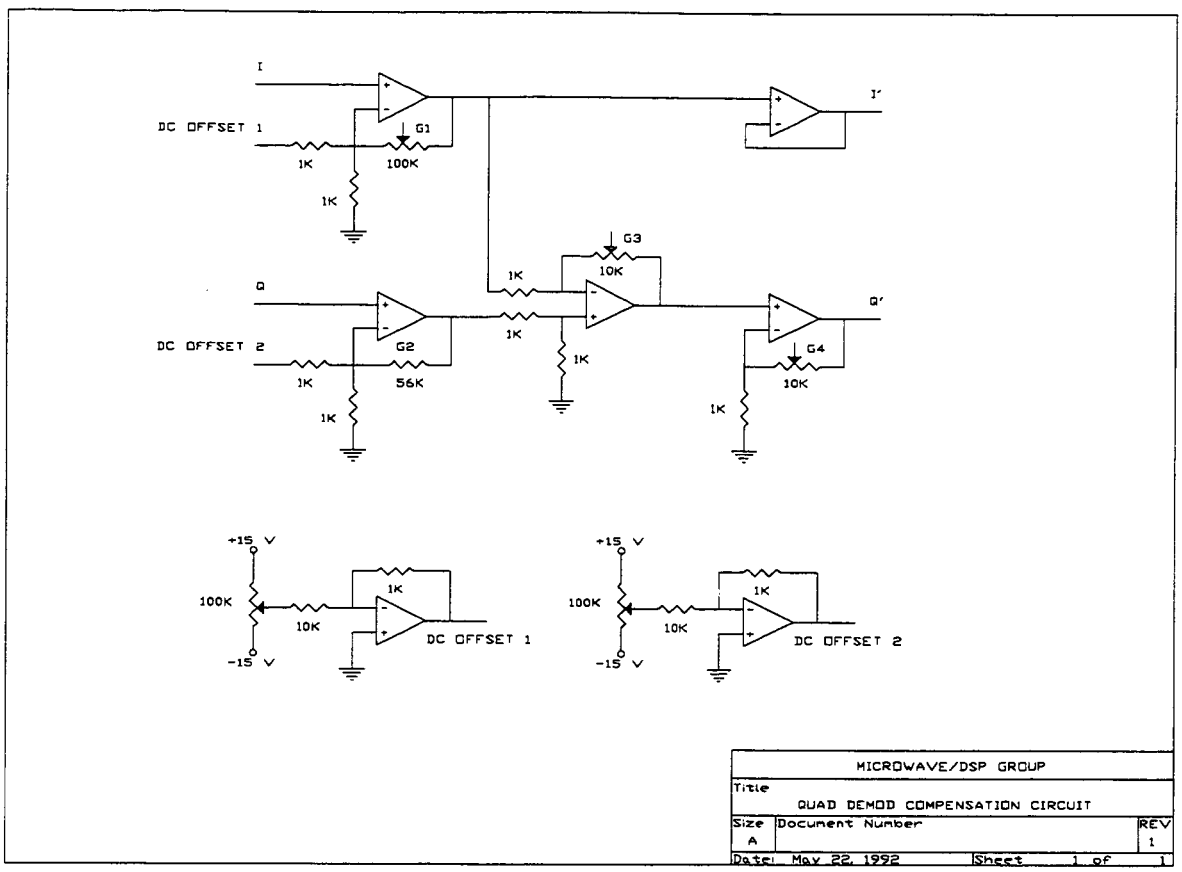

Figure A.2 Quad demod compensator circuit

A.3 Reconstruction Filter 1

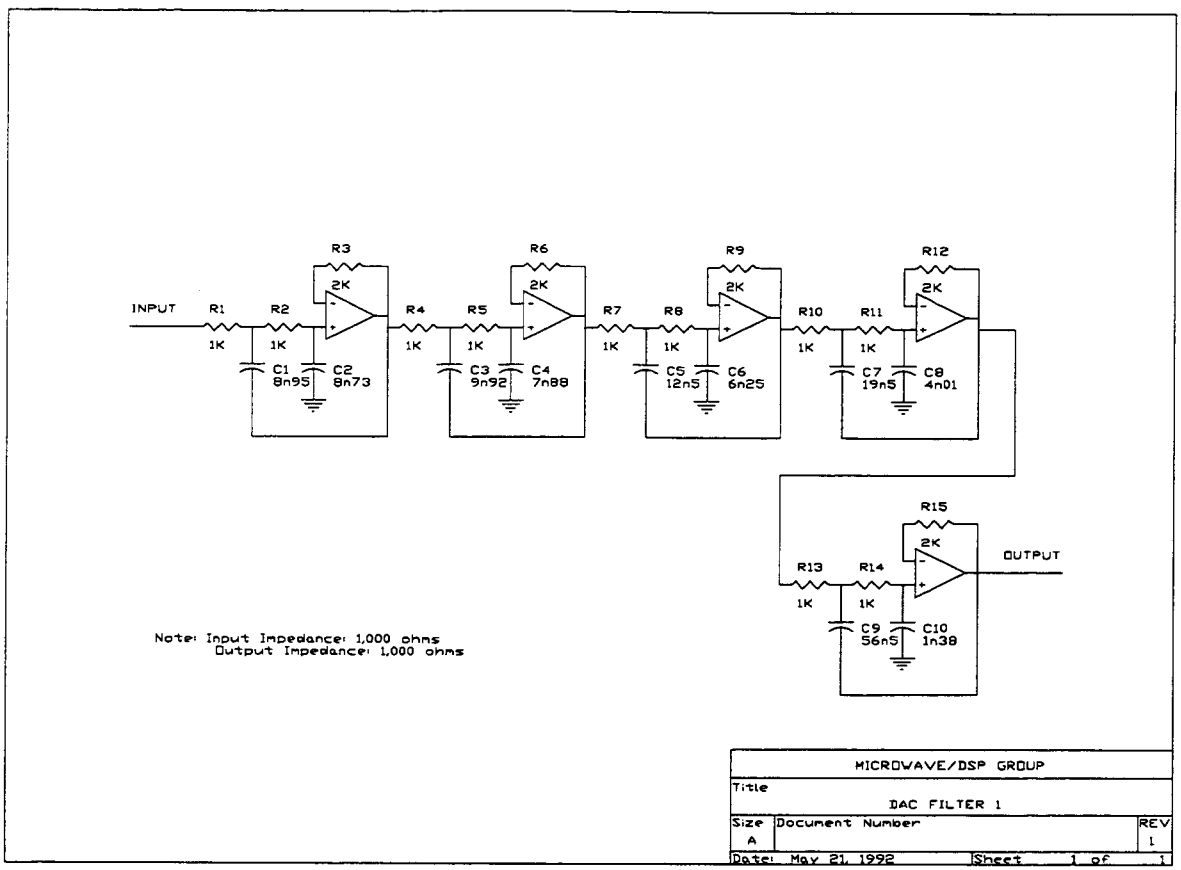

Figure A.3 Reconstruction filter 1

A.4 Reconstruction Filter 2

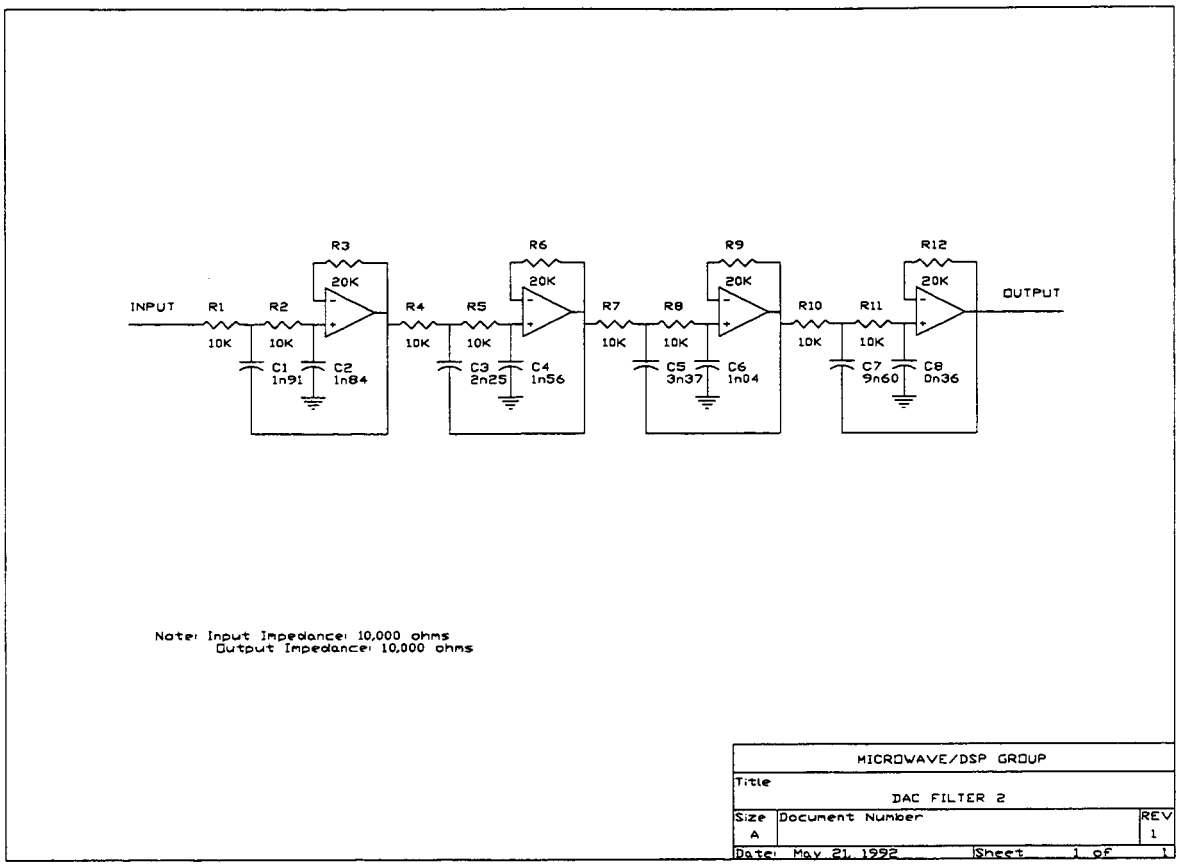

Figure A.4 Reconstruction filter 2

A.5 Anti-aliasing Filter

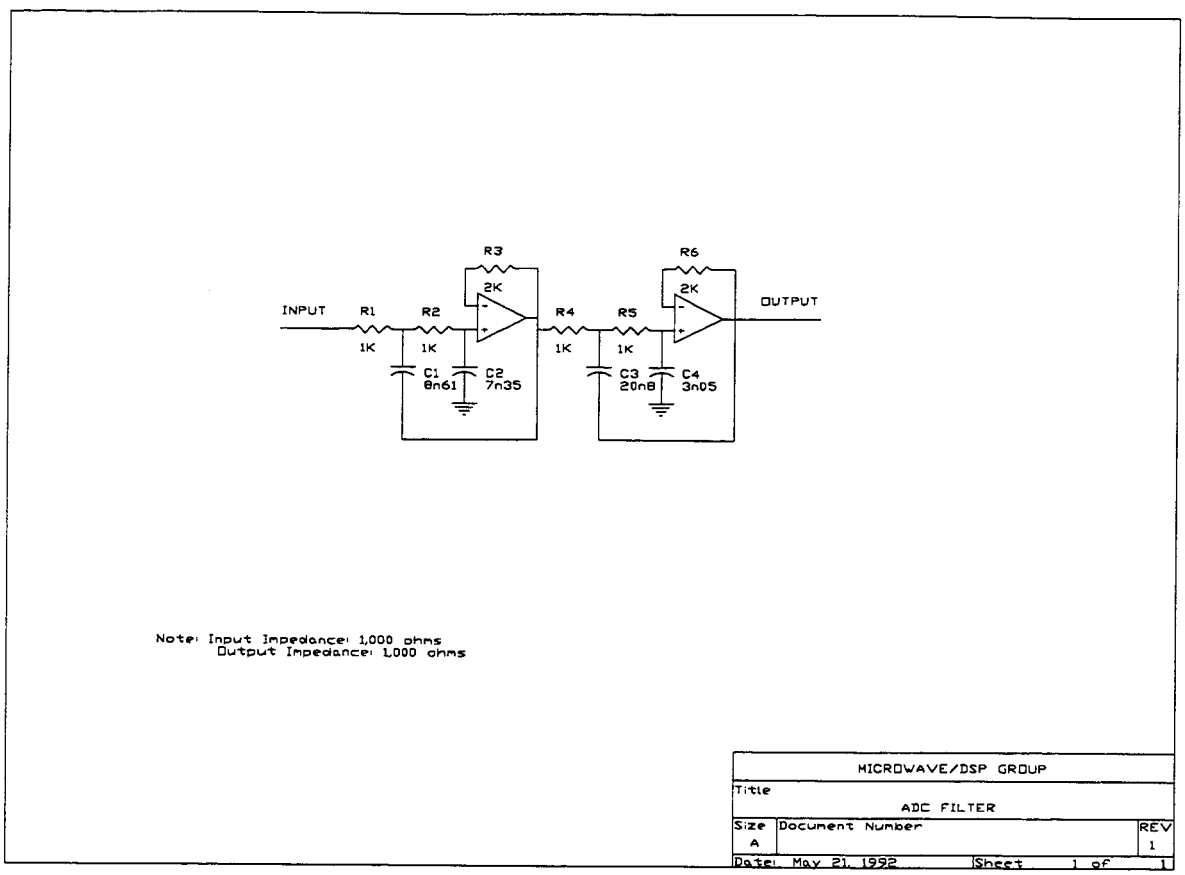

Figure A.5 Anti-aliasing filter

APPENDIX B

DERIVATION FOR QUAD DEMOD COMPENSATION

This appendix derives the compensation model for a quadrature demodulator (QUAD DEMOD). Mismatch in components used to build the QUAD DEMOD causes DC offsets, gain imbalance and phase imbalance in the demodulated signals. Figure B shows the model for a practical QUAD DEMOD with DC offsets a_1 and a_2, gain imbalance α, and phase imbalance φ.

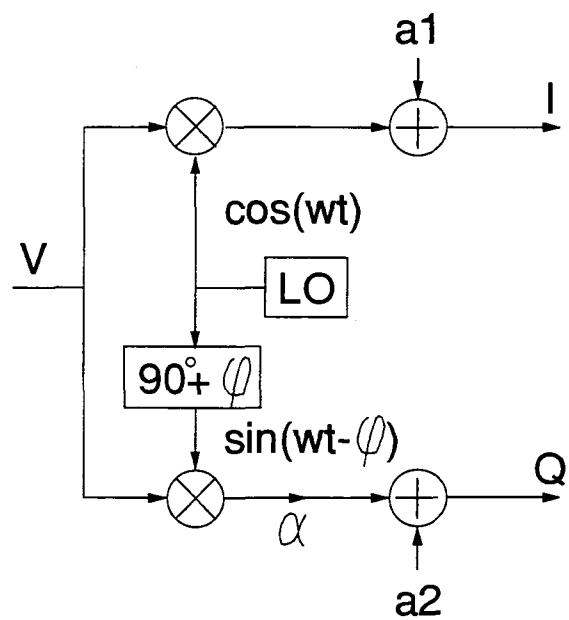

Figure B Model of a practical quadrature demodulator

As depicted in Figure B, the in-phase I and quadrature Q outputs are

$$I = v\cos(\omega t) + a_1 \tag{B.1}$$

$$Q = v\sin(\omega t - \varphi) + a_2$$

Or expressed in matrix form

$$\begin{bmatrix} I \\ Q \end{bmatrix} = \begin{bmatrix} 1 & 0 \\ -\alpha\sin\varphi & \alpha\cos\varphi \end{bmatrix} \cdot \begin{bmatrix} I_o \\ Q_o \end{bmatrix} + \begin{bmatrix} a_1 \\ a_2 \end{bmatrix} \tag{B.2}$$

where $I_o = v\cos(\omega t)$ and $Q_o = v\sin(\omega t)$ are the desired outputs. Solving for I_o and Q_o results in

$$\begin{bmatrix} I_o \\ Q_o \end{bmatrix} = \begin{bmatrix} 1 & 0 \\ \tan\varphi & \dfrac{1}{\alpha\cos\varphi} \end{bmatrix} \cdot \begin{bmatrix} I - a_1 \\ Q - a_2 \end{bmatrix} \tag{B.3}$$

Equation (B.3) describes the input-output relationship of the QUAD DEMOD compensator (QDMC). The compensation model can be divided into two sub-blocks, a DC compensator followed by a gain and phase compensator. That is, let

$$\begin{aligned} I' &= I - a_1 \\ Q' &= Q - a_2 \end{aligned} \tag{B.4}$$

And (B.3) can be expressed as

$$\begin{aligned} I_o &= I' \\ Q_o &= \frac{1}{\cos\varphi}\left(\frac{1}{\alpha}Q' + I'\sin\varphi\right) \end{aligned} \tag{B.5}$$

A model for the QDMC according to (B.4) and (B.5) is shown Figure 7.6.

APPENDIX C

DERIVATION FOR CONVERTER PHASE SHIFT

This appendix describes the phase shift resulted in the modulation and demodulation processes when there is a delay block in between these processes. Figure C depicts the described processes in which a lowpass filter introduces a delay of D samples.

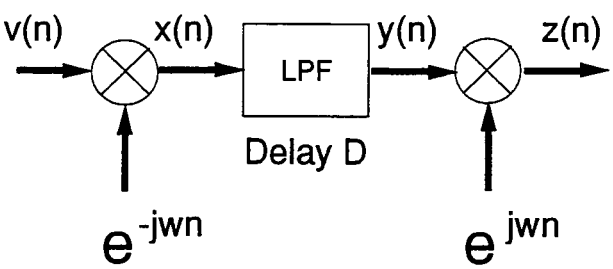

Figure C. Modulation and demodulation with delay block

The output sequence $x(n)$ of the modulator is

$$x(n) = v(n)e^{-jwn} \tag{C.1}$$

where $v(n)$ is the bandlimited input sequence, and $w = 2\pi \cdot \Delta f \cdot T_s$ is the discrete frequency with channel separation Δf and sampling period T_s.

Assume that the lowpass filter is ideal, and consider only the delay effect of the filter. The lowpass filter output is

$$\begin{aligned} y(n) &= x(n-D) \\ &= v(n-D)e^{-jw(n-D)} \end{aligned} \tag{C.2}$$

The output sequence $z(n)$ of the demodulator is

$$
\begin{aligned}
z(n) &= y(n)e^{jwn} \\
&= v(n-D)e^{-jw(n-D)}e^{jwn} \\
&= v(n-D)e^{jwD}
\end{aligned}
\tag{C.3}
$$

The output is a delay version of the input plus a phase shift, wD radians. To compensate for this phase shift, one can delay the output of the second LO by D samples; that is, using the LO of *ejw(n-D)* instead of *ejwn*. The resulted output is

$$
\begin{aligned}
z'(n) &= y(n)e^{jw(n-D)} \\
&= v(n-D)e^{-jw(n-D)}e^{jw(n-D)} \\
&= v(n-D)
\end{aligned}
\tag{C.4}
$$

Another way to compensate for that phase shift, is to designing the LPF such that with its delay D the resulted phase shift is a multiple of 2π; therefore the phase shift effect is transparent. The implementation presented in Section 7.3.4 employed this approach. For the given channel separation of 5 kHz, sampling frequency of 25 kHz, and filter delay of 10 samples, the resulted phase shift is 4π.